Ph.D. DISSERTATION

A Study on the Liquid Crystal Polymer-Based Intracochlear Electrode Array

액정 폴리머 기반 인공와우 전극에 대한 연구

BY

KYOU SIK MIN

FEBRUARY 2014

DEPARTMENT OF ELECTRICAL ENGINEERING AND COMPUTER SCIENCE
COLLEGE OF ENGINEERING
SEOUL NATIONAL UNIVERSITY

A Study on a Liquid Crystal Polymer-Based Intracochlear Electrode Array

액정 폴리머 기반 인공와우 전극에 대한 연구

指導敎授 金 成 俊

이 論文을 工學博士 學位論文으로 提出함

2013年 10月

서울大學校 大學院

電氣컴퓨터 工學部

閔 奎 植

閔 奎 植의 工學博士 學位論文을 認准함

2013년 12월

委 員 長 : _____

副委員長 : _____

委 員 : _____

委 員 : _____

委 員 : _____

Abstract

Owing to the chemical stability, low water absorption rate and low water vapor transmission rate, liquid crystal polymer (LCP) is considered a good material for neural interfaces where long-term reliability in an aqueous body environment is required. Several studies of LCP-based neural interfaces using micro-fabrication processes such as photolithography, thermal bonding and laser machining have been reported. These studies employed pre-opened cover LCP film with high melting temperature (high-temp LCP) as an encapsulation. The micro-sized metal patterns were deposited also on the high-temp LCP. An LCP layer with low melting temperature (low-temp LCP) was used as a bonding layer between high-temp LCP films. Subsequently, the bonded films were cut by laser machine with automated alignment setup. However, the resolution of the micro-sized lead wires was only 50-μm-wide with 100-μm-wide pitch, which did not fully utilize the advantages of micro-fabrication process. Moreover, the alignment error of laser machining process was not defined.

First, in the present study, we report advances in fabrication methods for LCP-based neural interface. Previous studies on LCP-based electrode arrays utilized photoresist for attachment of an LCP film to a

silicon wafer. The flatness of the aforementioned LCP coated wafer worsened due to the bubbles caused by solvent in photoresist, resulted in low resolution of photolithography process. In contrast, we employed a novel LCP film preparation process using silicone-elastomer-coated silicon wafer. The substrate prepared by suggested method enabled 10-μm-wide lead wires with 20-μm-wide pitch. Laser machining and lamination alignment errors were defined for optimization of electrode designs.

Secondly, we developed a highly flexible intracochlear electrode array using the micro-fabrication process stated above. The first LCP-based cochlear electrode array was reported in 2006, however, it was too stiff to be applied in human clinical use. The thickness and number of layers might affect its stiffness. In this study, we used two LCP layers for 16-channel electrode array. The thickness of single LCP film was 25 μm, which was half of single LCP layer of previously reported LCP-based intracochlear electrode array. The thickness of the finalized LCP-based electrode array was one-fifth of that of previous LCP-based intracochlear electrode array. For higher flexibility, the LCP substrate remained such a minimal extent as only to maintain lead wires. To protect the cochlear tissues from sharp edges of the LCP-film-based electrode array, we encapsulated the LCP-based electrode array using medical grade silicone elastomer. For this, a novel

micro-molding process employed self-alignment scheme was demonstrated. The diameters of the finalized electrode arrays were 0.5 mm (tip) and 0.8 mm (base). And the length was 28 mm.

Lastly, to assess the feasibility of the developed intracochlear electrode array in human clinical use, we investigated electrochemical and mechanical properties. The charge storage capacity and impedance at 1 kHz were 38.0 mC/cm^2 and 391 Ω, respectively. The insertion force into a transparent plastic cochlear model with displacement of 8 mm from a round window was 8.2 mN, and the maximum extraction force was 110.4 mN. In the human temporal bone insertion trial, the insertion depths were measured as 405°. Two cases of human temporal bone insertion showed no observable trauma while three cases showed a rupture of the basilar membrane.

Keywords: cochlear implant, liquid crystal polymer, intracochlear electrode array, implantable package, flexible neural interface, polymer based neural prosthesis

Student Number: 2009-30914

Contents

List of Figures

List of Tables

Chapter I

Introduction

1.1 Overview of Neural Prostheses

Neural prostheses are a series of medical treatment which replaces damaged sensory or motor function due to diseases or injuries by mimicking the target system. Sensory neural prostheses, such as cochlear implants and visual prostheses, deliver electrical stimulation to ganglion cells in cochlea or retina according to received sound or visual signal. On the other hand, functional electrical stimulation systems are used so as to restore function of nerves and muscles which have been paralyzed mainly due to spinal cord injuries. While functional electrical stimulation is a treatment for existing paralyzed limbs, motor prosthesis controls prosthetic limbs by processing an ensemble of neural signal recorded from brain cortex. Besides, bladder control and respiratory prostheses are available as neural prosthetic applications. Unlike the neuromodulation which uses electrical stimulation to treat pain, tremors, or neurological disorders using programmed stimulation patterns, the neural prostheses processes input signal to control the stimulation parameters or stimulation site.

Current commercialized cochlear implants, a representative neural prosthetic device, commonly consist of an external sound processor and an implant. The external processor collects the sound and divides it into several frequency bands. This signal is modulated and is transmitted through transcutaneous RF-link. The implant is made up of a wire-based platinum alloy electrode array, a receiver coil, electronics and a titanium based package. The electrode array is inserted into scala tympani to electrochemically interface with the spiral ganglion cell. The

electrode array consists of electrodes delivering electrical charge to the ganglion cell, lead wires and silicone carrier encapsulating the wires and electrodes. The electrical stimulation is delivered from the electronics encased in the titanium based package. Because general implantable package is made of electrically conductive titanium alloy or ceramic housing, feedthroughs should be employed to deliver electrical stimulation to multiple sites selectively. As non-conducting ceramic material is utilized for insulation of multi-channel feedthroughs, hetero-junction process accompanying ultra-high temperature should be applied to form hermetic sealing between ceramic and metallic materials. Likewise, other neural prosthetic devices consist of aforementioned components. Because most of aforementioned processes are manually handled, which result in low yield and high cost, major neural prosthetic device companies make efforts to develop manufacturing processes for higher efficiency and manufacturability.

1.2 Biomaterials for Neural Prostheses

Biocompatibility is an ability of a biomaterial to perform its desired function with respect to a medical therapy, without eliciting any undesirable local or systemic effects in the recipient or beneficiary of that therapy, but generating the most appropriate beneficial cellular or tissue response in that specific situation, and optimizing the clinically relevant performance of that therapy [1, 2]. In case of the neural prosthesis, the term is applicable to the substrate of neural interface and packaging material. Likewise, besides the immune response of a material,

mechanical property of target tissue should be considered for specific application. For example, in case of a neural probe, appropriate stiffness is needed for insertion of the electrode through the dura mater. On the other hand, an electrode array for surficial cortex application or a cuff electrode for nerve fascicles needs high flexibility. In this study, we focus on flexible materials as a substrate of neural interface.

1.2.1 Silicone Elastomer

Silicone refers to a polymeric material which has Si-O inorganic backbone. As depicted in figure 1.1, while the R component is usually represented as Me (polydimethylsiloxane, PDMS), the silicone can be modified to be suitable for aerospace, electronics, optics and medical applications by replacing R with phenyl, vinyl or trifuropropyl.

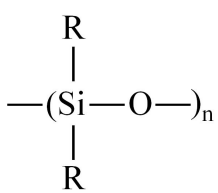

Figure 1.1 Si-O Inorganic backbone of Silicone. While the R component is usually represented as Me (polydimethylsiloxane, PDMS), the silicone can be modified to be suitable for aerospace, electronics, optics and medical applications by replacing R with phenyl, vinyl or trifuropropyl.

Silicone elastomer, polymerized to have ductility, has similar property with rubber. It is chemically inert and easily formable through injection molding. Silicone elastomer has many uses in artificial bio-tissues for implantation [3]. PDMS is also used as a substrate material for electrode array for recording of bio-signal [4, 5]. Its viscoelastic property is useful to fabricate a micro-molded structure or a deformable thin micro-electrode array.

1.2.2 Parylene-C

The term “parylene” is a generic name of chemical-vapor-deposited polymers based on polyxylylene (p-xylylene). Parylenes are used as variety of application due to their different properties according to the form of Di-p-xylylene. Among them, parylene-N, parylene-C, and parylene-D are most frequently used. As described in figure 1.2, Parylene-N refers to natural p-xylylene while parylene-C and parylene-D have one and two chlorine atom for aromatic hydrogen at the central benzene ring, respectively. This difference make the parylene-N have relatively high dielectric permittivity, the parylene-D have heat-resistance, and parylene-C have lower moisture absorption rate. Thus, parylene-C is used for bio-implantable application.

Parylene is usually used for insulation of electric circuit because of its high dielectric permittivity. Deposited parylene layer has excellent film quality, and its thickness is controllable by varying the deposition time according to the deposition rate. Having excellent film quality and low water absorption rate, it is used as a

coating material for stent or a substrate for retinal electrode [6].

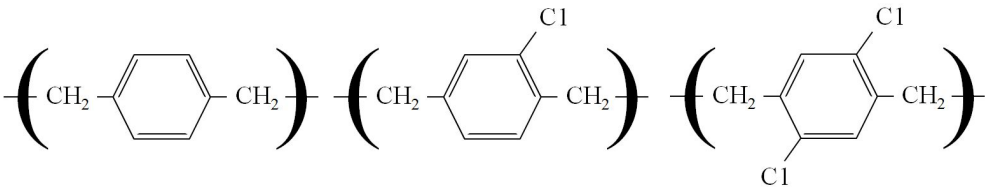

Figure 1.2 Dimers of Parylene-N (left), Parylene-C (center), and Parylene-D (right). Parylene-N refers to natural p-xylylene while parylene-C and parylene-D have one and two chlorine atom for aromatic hydrogens at the central benzene ring, respectively.

1.2.3 Polyimide

Polyimide is a polymer composed of imide monomers (figure 1.3). This yellow material is mechanically robust. It has high thermal resistance so that its high tensile force is maintained in a temperature as high as 232 °C with low thermal deformation. Molded polyimide can be used in a temperature as high as 260 °C. Polyimide has good chemical resistance that it is used as a substrate and an encapsulation material for implantable neural interface [7, 8]. Polyimide-based retinal electrode array or planar cortical electrode array is fabricated by micro-fabrication process. In the process, polyimide-resin-coated silicon wafer is used. The thickness can be controlled from microns to tens of micron by varying the revolution speed of spin coater. The polyimide is not affected by solvent, oleaginous solution, or diluted acidic solution. However, long-term reliability levels are controversial on account of their high moisture absorption rates and due to the unstable adhesion between the laminated layers in the body environment,

which contains corrosive fluids [9, 10]

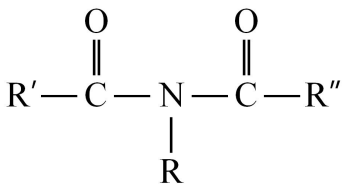

Figure 1.3 Imide Monomer. Polyimide is a polymer composed of imide monomers.

1.2.4 Liquid Crystal Polymer

Liquid crystal polymer (LCP) is a kind of aromatic polyester. It has so low reactivity that it has excellent chemical resistance even in the high temperature. The liquid crystalline structure can be formed by dissolving the polymer in solvent or heating the polymer above its melting temperature. The chain structure between solid monomer and soft monomer enables the LCP molecules to be arranged consistently even in aqueous state (figure 1.4). LCP is thermoplastic polymer which can be formed in high temperature. Its coefficient of thermal expansion is 0~30 ppm/°C which can be controlled to be less than that of polyimide, 20 ppm/°C. Moisture absorption rate of LCP is 0.02 % while that of polyimide is 2.8 %. LCP is biocompatible material which is USP class VI compliant and meets majority of ISO 10993-biological evaluations of medical devices for FDA approval [11]. (Table 1.1)

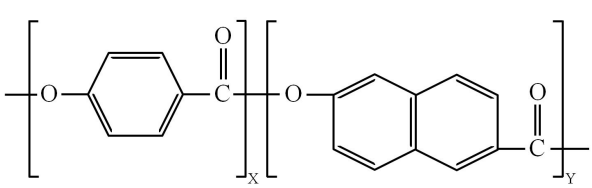

Figure 1.4 Crystalline Unit of LCP. The chain structure between solid monomer and soft monomer enables the LCP molecules to be arranged consistently even in aqueous state.

Table 1.1 ISO 10993 Tests for Implantable Medical Devices and Compliance of LCP to the Tests.

10993	Test	Compliance of LCP
5	Cytotoxicity	○ [11]
10	Sensitization	○ [11]
10	Irritation or Intracutaneous Reactivity	○ [11]
11	Systemic Toxicity (acute)	○ [11]
	Subchronic Toxicity (Subacute Toxicity) Up to 10% of life span of test animal	Have Not Been Tested
3	Genotoxicity	Have Not Been Tested
6	Implantation	○ [11, 12]
	Chronic Toxicity	○ [12]
3	Carcinogenicity	Have Not Been Tested

1.3 Liquid Crystal Polymer-Based Micro-Fabrication for Neurotechnology

Due to its good mechanical and chemical stability, liquid crystal polymer (LCP) is considered as a good candidate material for manufacturable biomedical

applications such as a neural electrode array and as an encapsulation material [13-19]. LCP has a much lower moisture absorption rate than those of polyimide and parylene-C, which is highly related to its long-term reliability [20-27]. The LCP material can also be employed as a near-hermetic packaging material for MEMS applications [28-30].

1.3.1 Neural Signal Recording

For neuro-technology application, LCP is firstly used as a neural signal recording electrode in 2004 (figure 1.5) [15]. The gold electrode array, lead wire, and contact pads were patterned by photolithography on an LCP layer. In the study, durability against heat and several chemicals, HF, HCl, H_2SO_4, HNO_3 and acetone, was evaluated to check the compatibility with semiconductor fabrication process, resulted in no changes in roughness and thickness. Evoked action potentials from a rat sciatic nerve were recorded by the electrode array. This work was meaningful as a first neural signal recording empolyed LCP based electrode array.

However, the lead wires as well as electrode contacts were exposed to outside because there was no encapsulation layer. Excessive exposure of electrode contacts including lead wires disturbs localized neural signal recording because the exposed lead wires are also affected by surrounding neural tissues. It was used for acute recording and the fabrication result was not appropriate for other application, such as neural stimulation because the electrodes and lead wires exposed to body-fluid would be dissolved by electrochemical reaction during stimulation. Thus, for chronic implantation of LCP based electrode array, an encapsulation layer should

have been employed.

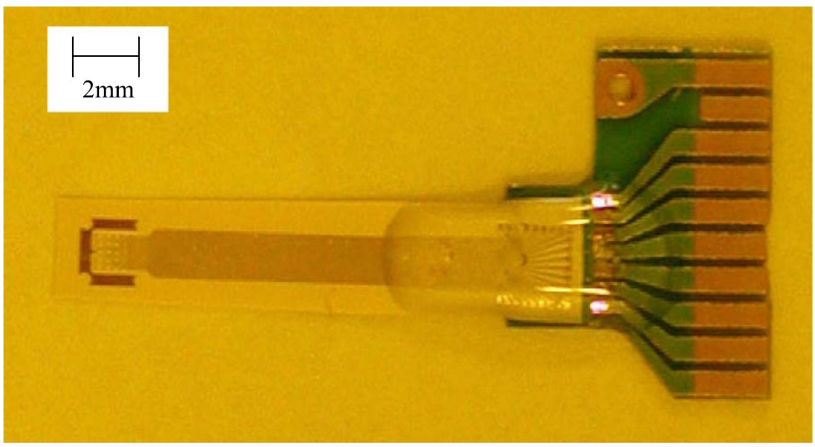

Figure 1.5 LCP-Based Neural Signal Recording Electrode Array [15]**.** Evoked action potentials from a rat sciatic nerve were recorded by the electrode array. This work was meaningful as a first neural signal recording employed LCP based electrode array. However, the lead wires as well as electrode contacts were exposed to outside because there was no encapsulation layer.

1.3.2 Electrode Array for Artificial Retinal Implant

LCP is usually used as substrate for printed circuit board (PCB). Its manufacturing properties, heat press bonding process, thermo-plasticity, low thermal expansion ratio, and so on, enable to develop multilayered flexible PCB. In 2009, an LCP-based microelectrode array for artificial retinal implant in the basis of aforementioned LCP-PCB manufacturing processes (figure 1.6) [17]. What made this work special was an encapsulation layer which was fusion-bonded by thermal press bonding process. For electrode contacts, the cover layer was pre-opened by laser cutting before the bonding process. No seam was observed at the

interface of the substrate and the cover layer. In vitro reliability test result showed that no sign of degradation of the interface was observed. The finalized electrode array was implanted in rat eye, and electrically evoked cortical potentials (EECPs) were recorded.

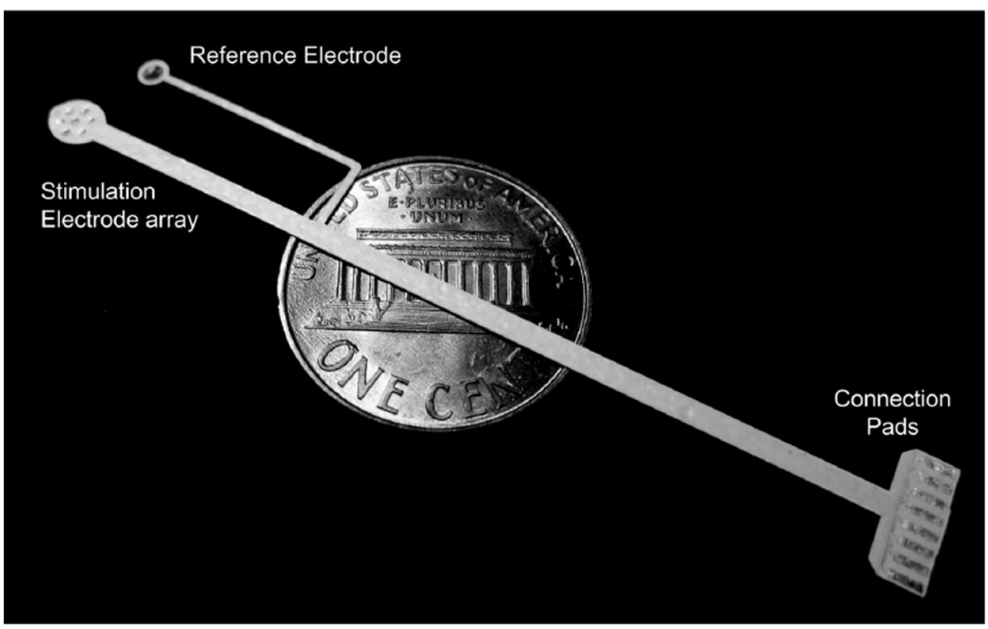

Figure 1.6 LCP-Based Artificial Retinal Implant Electrode Array [17]. In 2009, an LCP-based microelectrode array for artificial retinal implant in the basis of aforementioned LCP-PCB manufacturing processes. However, the number of channel was eight, which did not fully utilize the advantages of micro-fabrication process.

The electrode array was soft enough to be implanted in the cornea. However, the number of channel was eight, which did not fully utilize the advantages of micro-fabrication process. The micro-fabrication compatibility of

LCP is strongly related to the flatness of the substrate. Conventionally, including this work, the LCPs were attached to a silicon wafer by a photoresist layer [14, 22]. However, bubbles caused by outgassing due to the organic solvent and photoactive compound (PAC) could form a rough surface over time, resulting in a low resolution of photolithography.

1.3.3 Neural Probe

Conventionally, silicon and silicon-on-insulator (SOI) were used as a substrate and an encapsulation material for neural probes for decades due to its mass-producible and micro-fabricable properties [31-36]. However, mechanical rigidity may cause undesirable damage because of the pulsatile movement of brain tissue against the silicon-based neural probe [37, 38]. Moreover, due to the brittleness of the substrate, silicon-based neural probe can be broken in pieces by mishandling. To overcome these drawbacks, polymer-based neural probes were suggested as alternatives [39, 40]. Aforementioned polymers, parylene-C and polyimide, were used as a substrate and an encapsulation material because of compatibility with semiconductor fabrication process and biocompatibility. Because the conventional biocompatible polymers used for neural probes had been too flexible to be inserted into brain tissue, additional reinforcement or specific insertion instrument had been employed so that flexible probe shanks had supported the insertion force [41, 42].

On the other hands, an LCP-based neural probe utilizing intrinsic mechanical property was developed in 2012 (figure 1.7) [43]. In the report, without

additional reinforcement or special insertion instrument for insertion, a neural probe was fabricated and was inserted into the brain tissues of rats. Through buckling tests, the LCP-based neural probe was proven to have appropriate mechanical property for depth probe. It was shown that the mechanical characteristic of LCP could be controlled by varying the thickness according to applications.

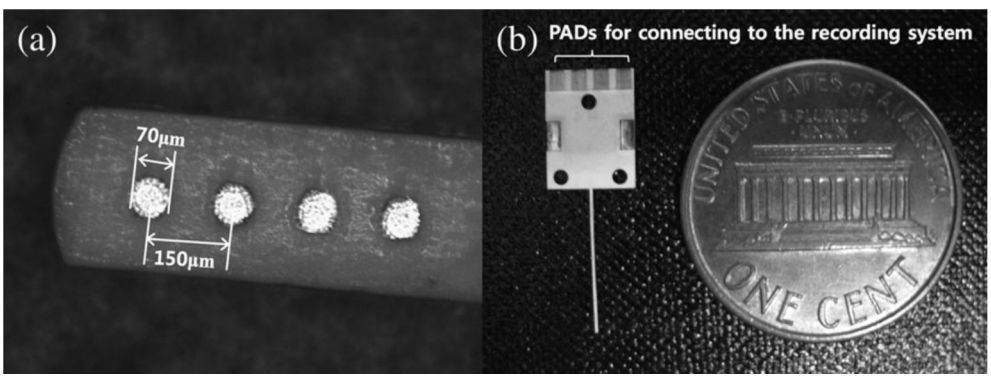

Figure 1.7 LCP-Based Flexible Neural Probe (a) Recording Site Array (b) Overall Structure [43]**.** Without additional reinforcement or special insertion instrument for insertion, a neural probe was fabricated and was inserted into the brain tissues of rats. It was shown that the mechanical characteristic of LCP could be controlled by varying the thickness according to applications.

1.4 LCP-Based Cochlear Electrode Array

The first LCP-based cochlear electrode array (figure 1.8) used 50-μm-thick LCP films [44]. Fine metal traces were patterned on LCP films with higher melting temperature (high-temp LCP). An LCP film with lower melting temperature (low-

temp LCP) was used as a boning layer in thermal press bonding of high-temp LCP layers. The electrode array had twelve electrode contacts at intervals of 200 μm. The length of the electrode array was less than 3 mm, and the apical dimensions of the finished electrode array were about 250 μm (W) × 250 μm (H). For better positioning of the electrode array near the cochlea, medical-grade silicone was employed as an overmold material of the LCP-based structure. It has been used in an acute animal trial [45], but the findings showed that it was too stiff for clinical use with humans.

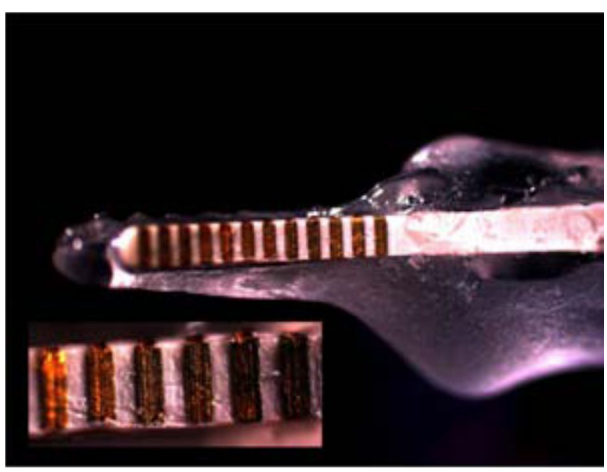

Figure 1.8 The First LCP-Based Cochlear Electrode Array [44]**.** The first LCP-based cochlear electrode array used 50-μm-thick LCP films. The length of the electrode array was less than 3 mm, and the apical dimensions of the finished electrode array were about 250 μm (W) × 250 μm (H). The findings showed that it was too stiff for clinical use with humans.

Table 1.2 LCP-Based Neural Prosthetic Devices.

Application	Results	Challenges Remaining
Neural Recording	Recording of Evoked Action Potential from Rat Sciatic Nerve	No Encapsulation
Artificial Retinal Implant	Monolithic Encapsulation and Its Long-Term Reliability	Low Resolution
Neural Probe	Neural Signal Recording from Brain Cortex and Appropriate Stiffness for the Application	Uniform Stiffness
Intracochlear Electrode	Used in Animal Acute Trial	Too Stiff for Clinical Use in Humans

1.5 Objectives of the Dissertation

In this study, we propose a fabrication process for microelectrode array with high-density interconnections. To realize ultra-fine line traces on an LCP substrate, a novel flattening method using silicone elastomer is suggested. The flatness total indicator reading (TIR) of the LCP surface attached to the silicon wafer using silicone elastomer was 16.0 μm, while the flatness of the LCP film attached using a photoresist layer was more than 43.7 μm. The alignment error of the thermo-press bonding was determined to be 84.4 ± 12.6 μm.

In this study, we suggested an LCP-based cochlear electrode array. The cochlear electrode array is fabricated by our previously reported fabrication process on a flexible LCP film [16, 17]. Because the thickness of the LCP is closely related to the stiffness of the electrode array, the high stiffness of the first LCP-based cochlear electrode array was likely caused by the thick LCP structure. The thickness of the present LCP electrode array was only 50 μm, which was thinner and more flexible than even one trace layer of the previously reported LCP-based cochlear electrode array. To gain more flexibility, in this study, an LCP substrate among the electrodes remained to such a minimal extent as only to maintain lead wires. Then, the LCP-based electrode array was molded in a silicone carrier. And, we demonstrated a novel self-aligning injection molding process. Instead of aligning each electrode on the mold manually [46, 47], we utilized a sawtooth-like structure of our LCP substrate to self-align and to open the electrode sites without an additional ablation process. The elastomer carrier encapsulated the sharp edges

of the LCP electrode so as not to destroy the surrounding tissues of the scala tympani. To assess the feasibility of the electrode array, the electrical and the mechanical characteristics of the finished electrode array were reported in this study. Human temporal bone study results were also presented. The objectives of the dissertation are as follows.

(1) A Suggestion of an Advanced Micro-Fabrication Process for LCP-Based Neural Prosthesis

(2) A Novel Injection Molding Method for Less Traumatic LCP-Based Neural Interface

(3) A Development of a Cochlear Electrode Array based on Suggested Fabrication Method and Its Evaluation

Chapter II

Materials & Methods

2.1 Design of an LCP-Based Intracochlear Electrode Array

Figure 2.1 (a) describes the structure of the LCP-based cochlear electrode array. It is fabricated by a laser micromachining, a customized thermal press and an injection molding. The conventional intracochlear electrode arrays are made up of platinum lead wires, electrodes and encapsulation. Among them, lead wires and electrodes are reinforcement of entire intracochlear electrode array because the young's modulus of the metallic structure is far greater than silicone rubber. Thus, the total stiffness of a conventional intracochlear electrode arrays are determined by lead wires and electrodes which are encapsulated in silicone elastomer.

Likewise, the LCP structure of suggested LCP-based intracochlear electrode array should be designed to reduce the stiffness. Conventional LCP-based electrode arrays utilized a high-temp LCP film as a substrate material for photolithography and a low-temp LCP film as a bonding layer. The minimal thickness of conventional method described in [44] is the sum of three layers of LCP films, high-temp LCP for substrate/ low-temp LCP for bonding/ high-temp LCP for encapsulation. In this study, however, the low-temp LCP films were used as both substrate and cover layers. In this way, we reduced the total thickness of the LCP-based electrode array, which is related to the stiffness.

Although LCP film is flexible along the normal direction of its surface, it is relatively rigid along the tangential direction. If a cochlear electrode is too rigid, it can cause damages to surrounding tissues. As shown in figure 2.1 (b), to reduce the rigidity along the z-axis (parallel to the modiolus), we reduced the width of the

LCP substrate between the stimulation sites. The width of the minimal extent for the lead wire was determined considering the alignment error in lamination process and laser machining process. To secure sufficient geometrical area of the stimulation electrode site, the shape of electrode array was machined as sawtooth structure (figure 2.2).

Electrode design consisted of three layers; metallization mask, cover window openings and laser machining outline (figure 2.2 (c)). The electrode contact sites were patterned in a rectangular shape of which width and height were 300 μm and 550 μm, respectively. Spacing between adjacent electrodes was 1.71 mm. At the corners of the mask design, the 500-μm-wide circular align keys for laser cutting were patterned. Design for site opening contains 280 μm and 530 μm site openings considering the width of laser-beam spot. In addition, openings for laser-machining align keys were also included. Because the outermost lead wire can be ablated by the laser in the final cutting process, the lines for laser cutting were drawn 100 μm apart from the outer most lead wire and sites.

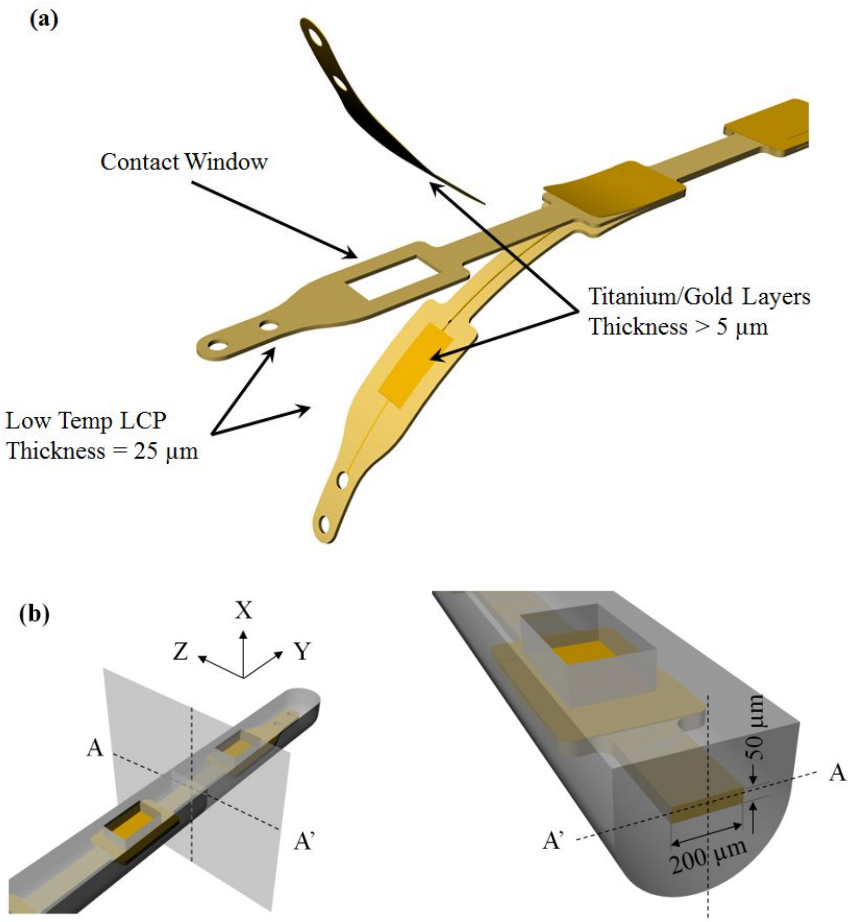

Figure 2.1 (a) 10um-wide metal wires and sixteen 300x550 μm^2 electrodes were patterned as interconnection lines and electrode sites on the LCP film (Kuraray, Vecstar FA-25, Tokyo, Japan) by photolithography and electroplating. Then, a laser-cut cover LCP layer and a patterned layer were laminated by a thermal-press bonding process. The final laser cut was followed by iridium oxide sputtering and an elastomer molding process. (b) The final laser cut was performed to reduce the rigidity along the z-axis, where the basilar membrane is. The aspect ratio of the cross-section of the interconnection part of the LCP electrode was 4:1 (apex) to 10:1 (base). This property made the electrode more flexible so that the electrode array does not destroy the basilar membrane.

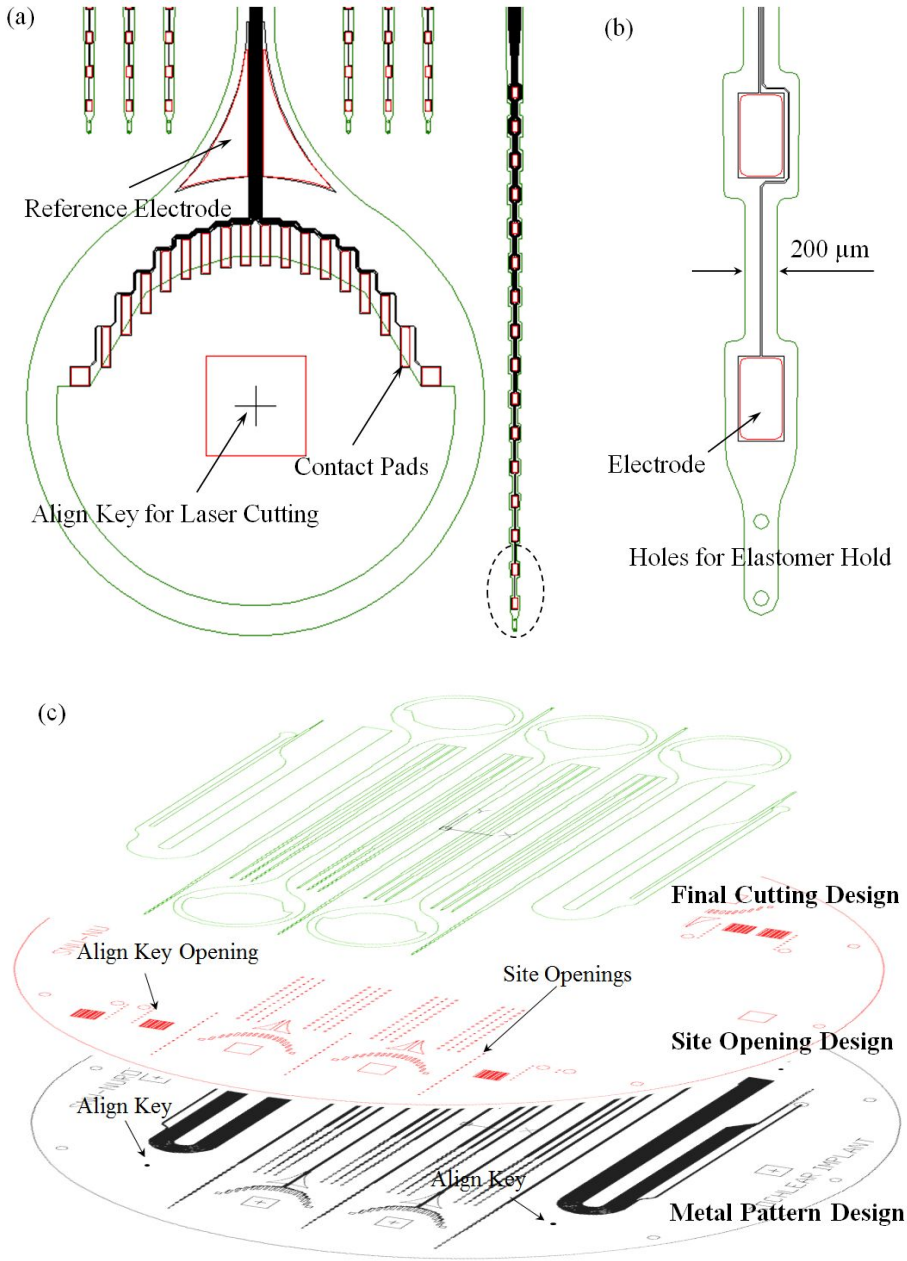

Figure 2.2 (a) Design of Electrode Array and Contact Pads. (b) Tip of the Electrode Array. To secure enough geometrical area of the stimulation electrode site, the shape of electrode array was machined as sawtooth structure. (c) Layer Designs. Layers consisted of designs for metallization mask, cover window openings and laser machining outline.

2.2 Advances in LCP-Based Micro-Fabrication Process

2.2.1 Preparation of a Flat LCP-Coated Silicon Wafer

Preparation process of a flat LCP-coated silicon wafer was depicted in figure 2.3. 3 ml of silicone elastomer (Nusil Silicone Technology, MED 6233, Carpinteria, CA, US) part A and part B were put into a 15 ml falcon conical tube. The silicone elastomer was mixed by a motorized drill tipped with spatula for 5 minutes. In succession, the mixed silicone elastomer was degassed in a centrifuge at 3000 rpm for 5 minutes. The silicone elastomer was poured on a 6-inch bare silicon wafer mounted on spin coater. Then, the silicon wafer was spun at 2000 rpm for 70 seconds. The silicone-elastomer-coated wafer was cured in a convection oven at 90 °C for 1 hour. A 25-μm-thick LCP film (Kuraray, Vecstar FA-25, Tokyo, Japan) was attached to the silicone elastomer by a roller. Residual LCP film out of the wafer area was cut by a drawing knife along the outline of the wafer. Then, one minute of consecutive cleaning processes in acetone, methanol and isopropyl alcohol were followed by the dry etching of the surface using an inductively coupled plasma (ICP) etcher for three minutes in an O_2 gaseous environment.

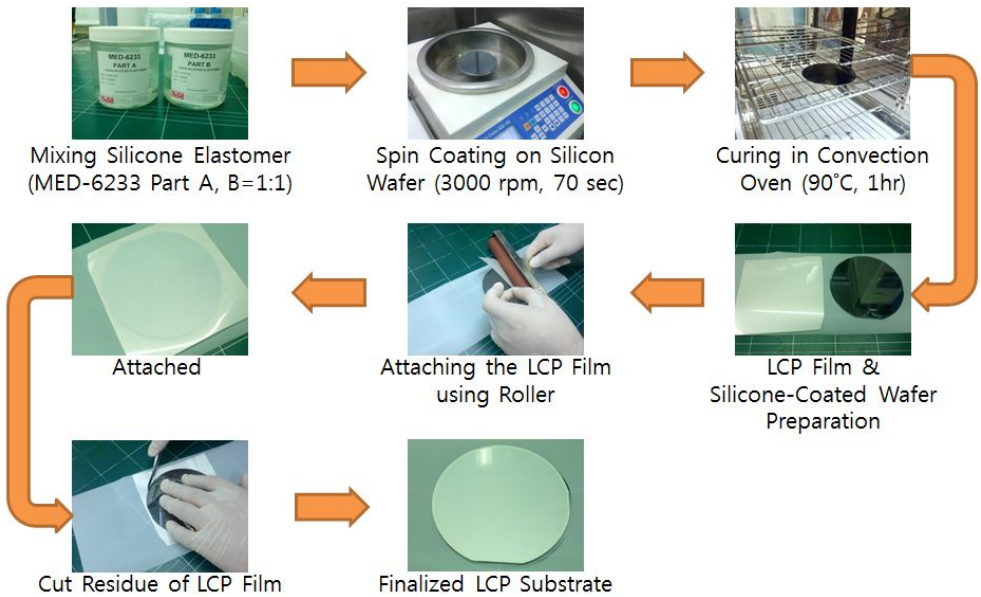

Figure 2.3 Preparation of Flat LCP-Coated Silicon Wafer**.** A silicon wafer was spin-coated by silicone elastomer (Nusil Silicone Technology, MED 6233, Carpinteria, CA, USA) at 2000 rpm for 70 seconds. The silicone elastomer was then cured in a convection oven at 90 °C for 1 hour. A 25-μm-thick LCP film (Kuraray, Vecstar FA-25, Tokyo, Japan) was attached to the silicone elastomer by a roller. Residual LCP film out of the wafer area was cut by a drawing knife along the outline of the wafer.

2.2.2 Photolithography

Subsequently, titanium and gold electroplating seed layers were deposited by an e-gun evaporator (Maestech Co., Ltd., ZZS550-2/D, Pyung Taek, South Korea) at 50 nm and 100 nm, respectively. Spin coating of hexamethyldisilazane (HMDS) on a spin coater at 500 rpm for 7.5 seconds and at 2500 rpm for 10 seconds was followed by spin coating of a photoresist (Clariant, AZ4620, Muttenz,

Switzerland) at 500 rpm for 10 seconds and at 2000 rpm for 40 seconds, results in 10-μm–thick photoresist layer. A soft bake process was performed on a hot plate at 110 °C for 80 seconds. And, after the photoresist-coated LCP-wafer was aligned beneath the photo-mask mounted on a mask aligner machine (SUSS MicroTec, MA6/BA6, Garching, Germany), the photoresist was exposed by ultra violet light source of 17 mJ/cm^2 for 70 seconds. The exposed sample was developed in a developer (Clariant, AZ 300 MIF, Muttenz, Switzerland) for 210 seconds. In the electroplating mold patterned on 10-μm-thick photoresist, gold was electro-plated by 5 μm. After the seed layer on the LCP substrate was etched in nitrohydrochloric acid and hydrofluoric acid, the substrate was detached from the elastomer-coated wafer.

Table 2.1 Photolithography Process.

Process	Condition
HMDS Coating	500 rpm for 7.5 sec → 2500 rpm for 10 sec
Photoresist Spin Coating	AZ 4620, 500 rpm for 10 sec → 2000 rpm for 40 sec
Soft Bake	110 °C for 80 sec
Aligning	Mask Aligner
Exposure	UV light Source, 17 mJ/cm^2 for 70 sec
Develop	AZ 300 MIF, for 210 sec
Electroplating	Gold, 5 μm Thickness

2.2.3 Lamination and Laser-Cutting

1-mm-diameter align holes for the substrate and the cover film (Kuraray, Vecstar FA-25, Tokyo, Japan) were laser-cut by a UV laser machining system (Electro Scientific Industries, Flex5330, Portland, OR, US). Besides the align holes, the laser-cutting design of the cover layer should include the outlines of the via-opening, the align key for the final laser cutting process and the contact pads. Lamination-align holes of the substrate and the cover layer were made in align columns on a customized aluminum press mold (figure 2.4 (g)). To avoid the unexpected bonding between press mold and LCP layer, 200-μm-thick Teflon® films were laid beneath the bottom and on the top of the LCP film layers. And, for uniform application of pressure to whole area of LCP surface, a 1-mm-thick ceramic cushion was placed on the top Teflon® film (figure 2.5(a)). Then, the press mold was placed between heat plates of the thermal press machine (Carver, Model 4122, Wabash, IN, US). The heat plates were heated to 285 °C at the rate of 7 °C/minute. While heating the plates, any pressure should not be applied to the press mold. At 285 °C, the mold was pressed for 40 minutes while maintaining the pressure at 500 kg (figure 2.5(b)).

A disposable shadow mask was also laser-cut on 100-μm-thick LCP film. Before extracting the thermally bonded LCP layers, the shadow mask was placed on the press mold and was aligned by putting an alignment holes on the mold. After fixing the shadow mask and laminated film with Kapton tape, a titanium layer and a gold electroplating seed layer were sputter-deposited as thick as 50 nm and 100 nm, respectively. The film was laser-cut along the outlines of electrode array, and

iridium oxide or platinum layers were electroplated through the contact pad.

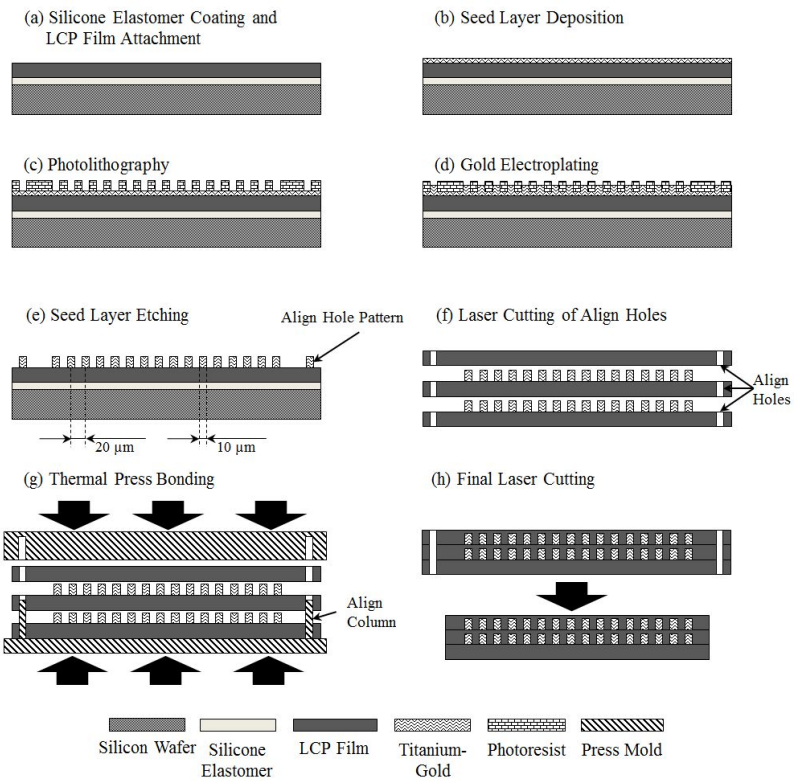

Figure 2.4 Micro-Fabrication Process Flow: (a) Silicone elastomer was spin-coated onto a silicon wafer and LCP film is attached by a roller. (b) After the cleaning of the film surface in O_2 plasma, a gold seed layer was deposited. (c) Leads, sites and align keys were patterned on a thick photoresist. (d) An electro-plating of gold of 5 µm. (e) The seed layer was wet-etched in nitrohydrochloric acid and hydrofluoric acid. (f) The align hole was drilled on the substrate and cover layer. Openings on the cover layer for the sites, vias, pads and align keys were also laser-cut. (g) On a customized aluminum mold, the substrate and the cover layer were aligned and thermally bonded. (h) Laser-cutting of the outline of the electrode array was then done.

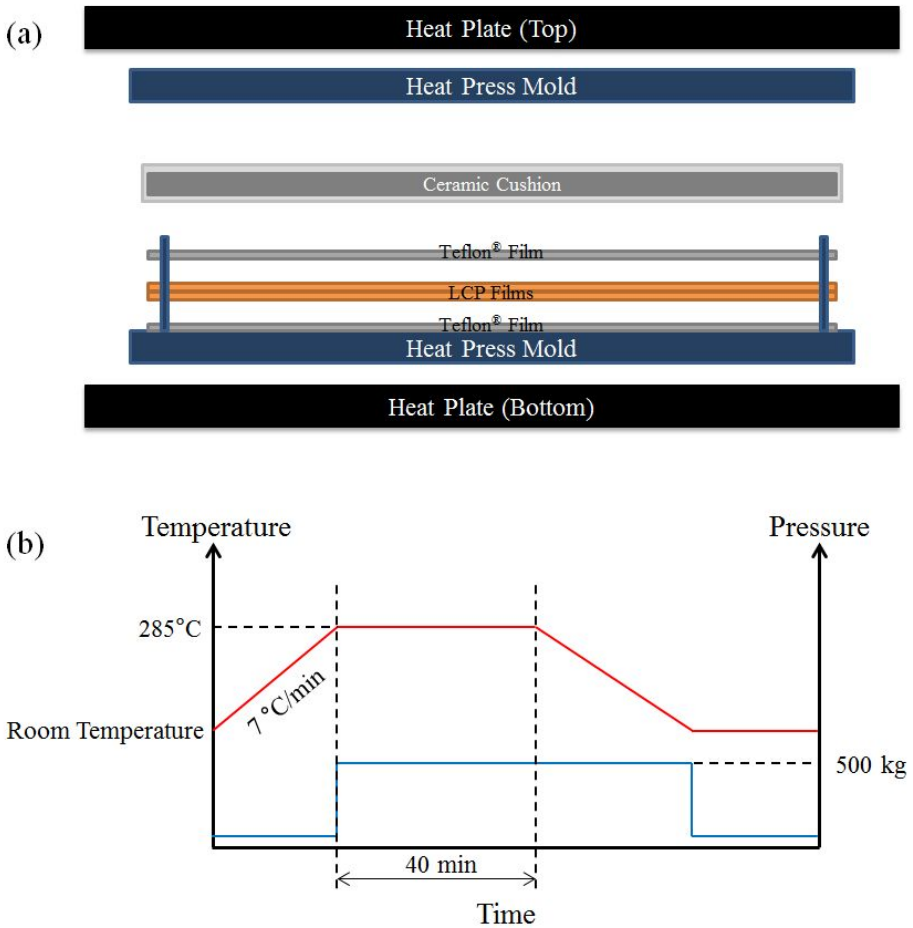

Figure 2.5 (a) Heat Press Bonding Setup. To avoid the unexpected bonding between press mold and LCP layer, 200-µm-thick Teflon® films were laid beneath the bottom and on the top of the LCP film layers. And, for uniform application of pressure to whole area of LCP surface, a 1-mm-thick ceramic cushion was placed on the top Teflon® film. (b) Temperature and Pressure Profile. The press mold was placed between heat plates of the thermal press machine (Carver, Model 4122, Wabash, IN, US). The heat plates were heated to 285 °C at the rate of 7 °C/minute. While heating the plates, any pressure should not be applied to the press mold. At 285 °C, the mold was pressed for 40 minutes while maintaining the pressure at 500 kg.

2.3 Silicone Encapsulation Using Self-Alignment Method

Because the sharp edges of the thin film substrate can also destroy cochlear tissue, we molded the thin film with silicone elastomer using a customized molding process. To open the electrode sites of a silicone-molded neural interface, oxygen plasma etching [48] or a laser ablation process had been usually employed [49]. However, we devised a molding process which opened the sites without an additional process. In this study, the stepwise injection molding process consisting of two steps was employed for self-alignment and site opening.

2.3.1 Mold Design

For micro-molding employing the self-alignment, a set of molds consisted of molds for bottom, LCP trench and site opening was designed. The design of bottom mold contained an electrode body, an inlet and four outlets. On the bottom mold, semicircular electrode body of which cross-sectional diameter at the tip and at the base were 500 μm and 850 μm, respectively. From the basal region, silicone elastomer was injected through a 2-mm-wide and 200-μm-deep inlet (figure 2.6 (b)). On the other side of the inlet, a semicircular outlet of which diameter was 100 μm. At the tip of the bottom mold, there were three outlets at the terminal and both sides of the terminal of the trench as depicted in figure 2.6 (c). The semicircular electrode body design was recessed by 200 μm from the surface of the mold to make a trench for LCP electrode array (figure 2.6 (d)). At the corners of the bottom mold, 5-mm wide align pins were placed. A cover mold for the self-alignment of

LCP electrode array was designed as figure 2.7 (a, c). The edges of the protruded structure were designed as same shape of the outline of LCP electrode array. The height of the structure was 200 μm. Thus, the result of cured silicone elastomer molded by this cover mold contains 200-μm-deep trench. On the cover mold, the silicone elastomer inlet was drilled as large as 2 mm in diameter. At the corners, there were align holes for align pins on bottom mold. Likewise, as described in figure 2.7 (b, d), the other cover mold contained pillars as many as the number of the electrode sites. The height of the each pillar was 200 μm. Because the height of the LCP electrode array was more than 50 μm and the depth of the trench was 200 um, the rectangular pillars pressed the electrode sites as deep as 50 μm after the joining of the bottom and the cover molds. Thus, the silicone elastomer injected from the basal region of the joined mold could not cover the electrode sites due to the structural contact between surfaces of electrodes and pillars.

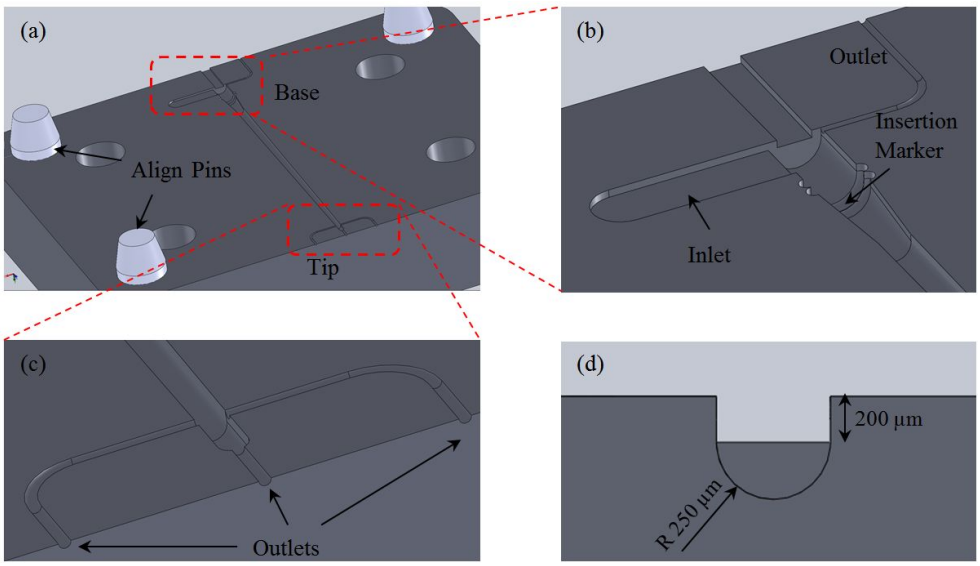

Figure 2.6 Bottom Mold Design. (a) Overview of the Bottom Mold. Semicircular electrode body was designed, of which cross-sectional diameters at the tip and at the base were 500 µm and 850 µm, respectively. (b) Enlarged Picture of Basal Region of the Bottom Mold. From the basal region, silicone elastomer was injected through a 2-mm-wide and 200-µm-deep inlet. (c) Enlarged Picture of Apical Region of the Bottom Mold. At the tip of the bottom mold, there were three outlets at the terminal and both sides of the terminal of the trench. (d) Cross-sectional View of the Apical Region of Trench for LCP Electrode Array. The semicircular electrode body design was recessed by 200 µm from the surface of the mold to make a trench for LCP electrode array.

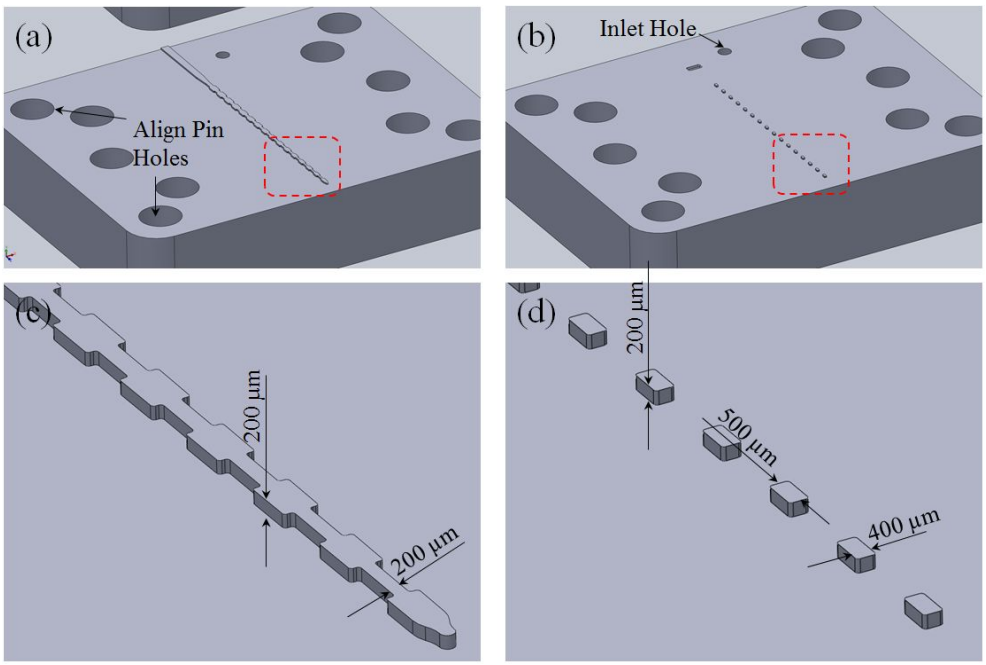

Figure 2.7 Cover Molds. (a) Cover Mold for Self-Alignment Trench. The edges of the protruded structure were designed as same shape of the outline of LCP electrode array. (b) Cover Mold for Electrode Encapsulation. The cover mold for electrode encapsulation contained pillars as many as the number of the electrode sites. (c) Enlarged View of the Cover Mold for Self-Alignment Trench. The result of cured silicone elastomer molded by this cover mold contained 200-µm-deep trench. (d) Enlarged View of the Cover Mold for Encapsulation and Site Opening. The silicone elastomer injected from the basal region of the joined mold could not encapsulate the electrode sites due to the contact between surfaces of electrodes and pillars.

2.3.2 Stepwise Injection Micro-Molding

In the first injection molding, the silicone elastomer (Nusil Silicone Technology, MED 6233, Carpinteria, CA, USA) carrier part was initially molded. As much as 1.5 ml of each silicone elastomer part (part A and part B) was taken into 5 ml injection barrel. Subsequently we mixed the silicone elastomer for 5 minutes using a motorized drill tipped with spatula. Too rapid rotation of the drill may cause excessive frictional heat, resulted in unexpected curing. Because the mixed silicone elastomer contained too many bubbles, degassing process was done in a centrifuge at 3000 rpm for 5 minutes. The base of the injection barrel was connected to a digital fluid dispenser (Techon Systems, TS250, Garden Grove, CA, US). The tip of the injection barrel was inserted at the inlet of the cover mold for self-alignment. The joining of cover mold and the bottom mold was followed by elastomer injection in 30 lbs/in^2. The injection pressure was maintained until the silicone elastomer was emerged at the outlets of apical region. If the elastomer was emerged at the outlets, the mold was placed on a hot plate of which temperature was 150 °C for 30 minutes. After the mold was cooled down to room temperature naturally, the cover mold was carefully disassembled from bottom mold so that the cured silicone elastomer was left in the bottom mold. This molded part did not contain an electrode array but instead had a 200-μm-deep guiding groove for an outline of the sawtooth-like LCP electrode array (figure 2.8 (a, e)). Because the outline of the guiding groove was designed based on the laser-machined microstructure of the LCP electrode array, each electrode site was self-aligned to be fixed in its position (figure 2.8 (b, f)). After the LCP electrode array was aligned

and was placed in the microstructure, the encapsulating silicone layer was molded by the cover mold for encapsulation and site opening, with precise alignment upon the electrode sites (figure 2.8 (c)). The silicone elastomer was injected into the mold consisted of bottom mold and cover mold for encapsulation. Because the pillars on the cover mold were in contact with and pressing the electrode sites, after the release, every stimulation site was open to the outside (figure 2.8 (d, g)).

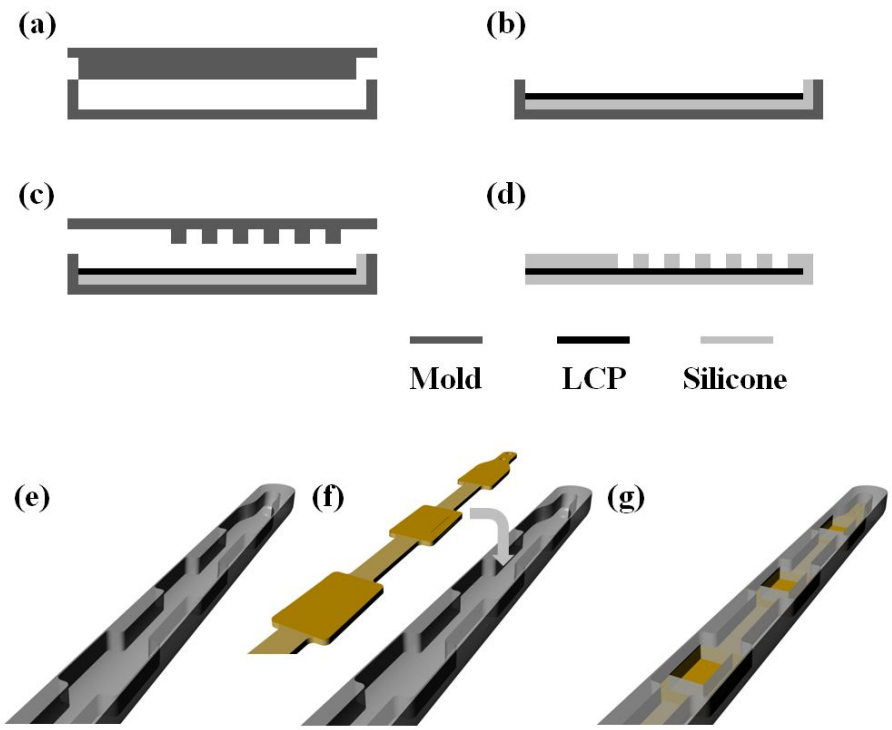

Figure 2.8 Thin Film Molding Process for Self-Alignment. A 200-µm-deep groove was initially molded along the outline of the LCP electrode array as an alignment pattern (a, e). The LCP electrode was positioned in the groove. Silicone rubber was mounted in the base mold used in the (a) and (b) processes (b, f). The cover silicone layer was molded with a cover mold with rectangular pillars upon the electrode sites (c-d, g). Without laser ablation or an oxygen plasma etching process, the electrode sites were opened successfully.

2.4 Evaluation

2.4.1 Evaluation of Micro-Fabrication Process

The flatness of a bare glass wafer, an LCP-attached wafer using a photoresist adhesion layer and an LCP-attached wafer using a silicone elastomer adhesion layer were measured by a wafer analysis system (Corning Tropel Corporation, FlatMaster® MSP-300, Fairport, NY, US). The results of the photolithography and electroplating of the lead wires were examined by a scanning electron microscope (SEM). The laser-cut LCP film was inspected under an optical microscope to measure the burnt area. Alignment errors after the lamination and laser-cutting processes were also calculated through measurement statistics.

2.4.2 Evaluation of the LCP-Based Cochlear Electrode Array

2.4.2.1 Electrochemical Property

Cyclic voltammetry was conducted to assess the charge storage capacity (CSC). The electrolyte was a phosphate-buffered saline (PBS) solution (Invitrogen Life Technologies, Gibco #10010, Carlsbad, CA, USA) at pH 7.2. Using a potentiostat (Solartron Analytical, 1287A, Farnborough, UK) and a three-cell electrochemical system with a platinum counter electrode and a silver/silver chloride (Ag/AgCl) reference electrode, we swept the electrochemical potential from -0.6~0.8V versus an Ag/AgCl electrode at a sweep rate of 100 mV/s. We also measured the electrochemical impedance spectrum using an impedance analyzer (Solartron Analytical, 1286 and 1287A, Farnborough, UK). We used an identical

electrochemical cell for the cyclic voltammetry measurements. The impedance spectrum was measured under a 10 mV_{rms} excitation at frequencies ranging from 0.1 Hz to 100 kHz

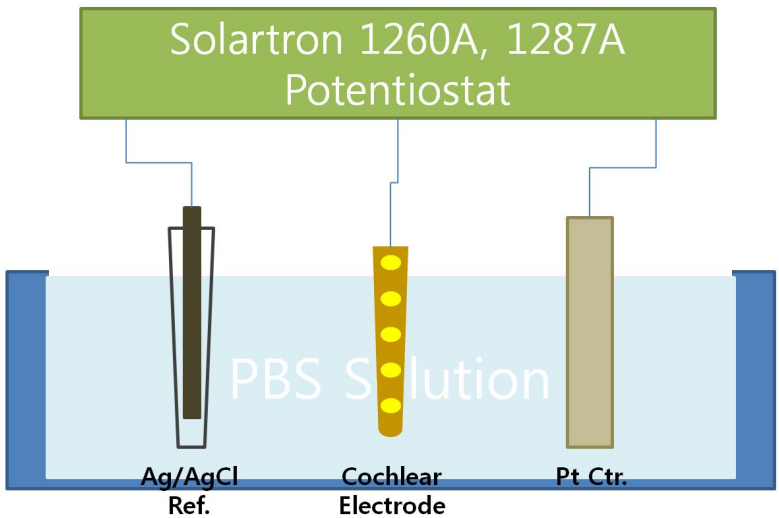

Figure 2.9 Electrochemical Analysis Setup**.** Using a Potentiostat (Solartron Analytical, 1287A, Farnborough, UK), impedance analyzer (Solartron Analytical, 1286, Farnborough, UK) and a three-cell electrochemical system with a platinum counter electrode and a silver/silver chloride (Ag/AgCl) reference electrode, we measured the charge storage capacity and electrochemical impedance.

2.4.2.2 Mechanical Property

The insertion characteristics and the final position of the electrode array in the scala tympani (ST) are becoming far more important in today's cochlear implant systems because conservation of residual hearing means an expansion of cochlear implant candidates [50-52]. In this study, the mechanical characteristics were measured by a method reported in earlier work [53]. The stiffness of the

finished electrode array was measured after fixing the electrode array in a custom-designed fixture. The stiffness of a 16-channel wire-based intracochlear electrode array used in the aforementioned study [53] was also measured in this fixture for comparison. This wire-based electrode array was manufactured by conventional method which employs manual handling. Each ball-shaped electrode sites was fabricated by melting the Teflon®-coated platinum (90%)-iridium (10%) wire with oxygen/acetylene mini-torch. The cross-sectional diameter of the wire was 75 μm. Thus, to obtain a ball electrode of which diameter was 420 μm, we melt the wire as long as approximately 3-mm. In this way, 16 electrodes and lead wires were fabricated and were prepared for silicone elastomer molding. As depicted in figure 2.10 (a, b), each ball-type electrode was fixed on 400-μm-wide holes which were drilled at the bottom of the mold. The interface between the ball and the mold was sealed by the medical grade silicone elastomer (Nusil Silicone Technology, MED 6233, Carpinteria, CA, USA) so that the electrode sites were not covered by silicone elastomer after the final molding process. After another ends of the lead wires were fixed by the silicone elastomer, degassed silicone elastomer was injected into the securely joined cover mold and the bottom mold with electrode array. The elastomer was cured for 30 minutes at 120 ˚C. The diameters of the wire-based electrode array were 600 μm at the apex and 800 μm at the base. The length of the wire-based electrode array was 21.5 mm and the distance between adjacent electrodes was 0.9 mm.

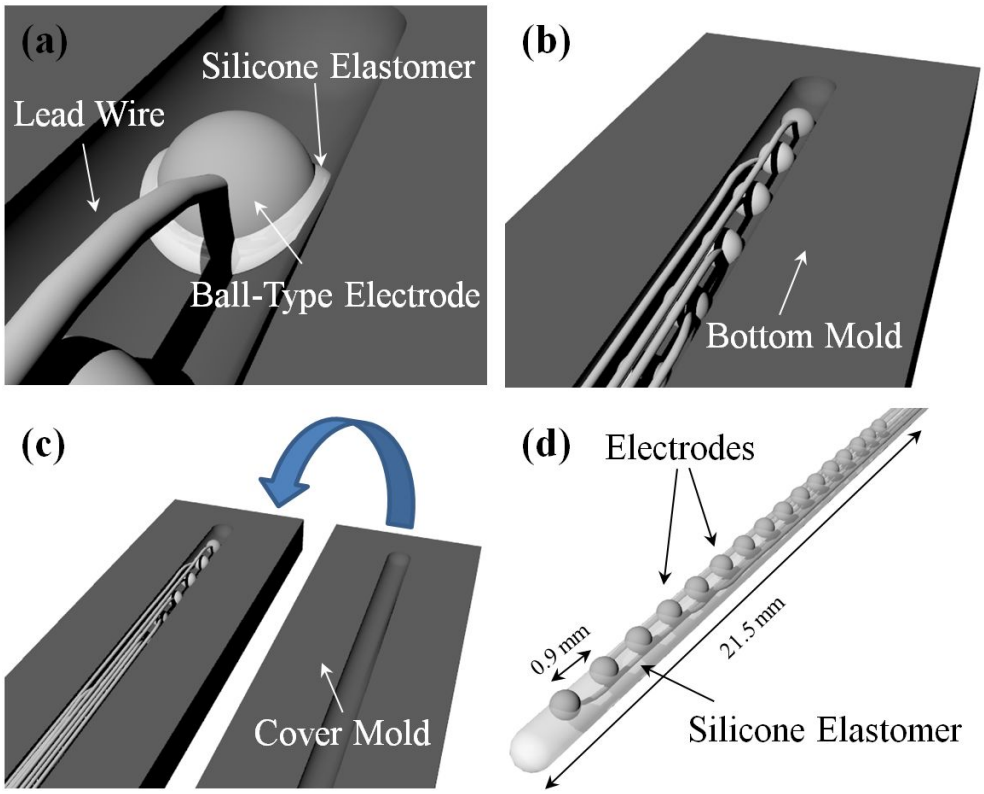

Figure 2.10 Fabrication Process of Wire-Based Ball-Type Intracochlear Electrode Array. (a) Ball-type electrode made from platinum/iridium alloy was fixed on 400-μm-wide hole drilled at the bottom of the mold by the medical grade silicone elastomer. (b) In this way, 16 electrodes were securely fixed on the bottom mold. (c) After another ends of the lead wires were fixed by the silicone elastomer, degassed silicone elastomer was injected into the securely joined cover mold and the bottom mold with electrode array. (d) The elastomer was cured for 30 minutes at 120 ˚C. The diameters of the finalized wire-based electrode array were 600 μm at the apex and 800 μm at the base. The length of the wire-based electrode array was 21.5 mm and the distance between adjacent electrodes was 0.9 mm.

Each electrode array (wire-based and LCP-based) was held securely and a mechanical force gauge measures the force needed to bend the array by 30° from its normal shape. Horizontal and vertical deflection forces were measured at every 1 mm spot from the bases of the arrays. The stiffness ratio was calculated by dividing the vertical deflection force by the horizontal deflection force (figure 2.11). The insertion force of the LCP-based electrode array was also compared to that of wire-based electrode array (figure 2.12). A load cell (ATI, Nano17, Pinnacle Park, Apex, NC, USA) was fixed to a motorized linear actuator (Newport, LTA-HS, Irvine, CA, US). The actuator was controlled by Labview® software, which also recorded the displacement and insertion force. For the insertion force measurements, 50% glycerin was used as a lubricant.

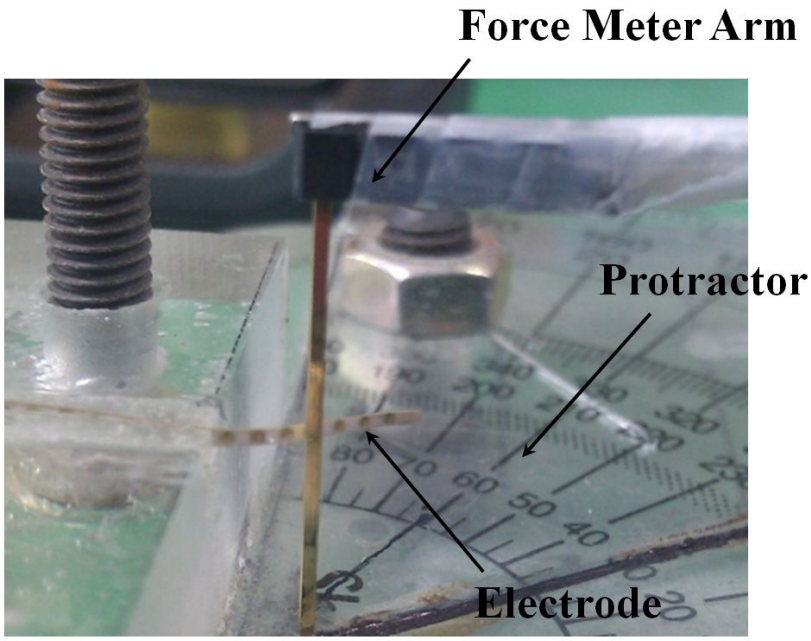

Figure 2.11 Deflection Force Measurement. Each electrode array (wire-based and LCP-based) was held securely and a mechanical force gauge measured the force needed to bend the array by 30° from its normal shape. Horizontal and vertical deflection forces were measured at every 1 mm spot from the bases of the arrays.

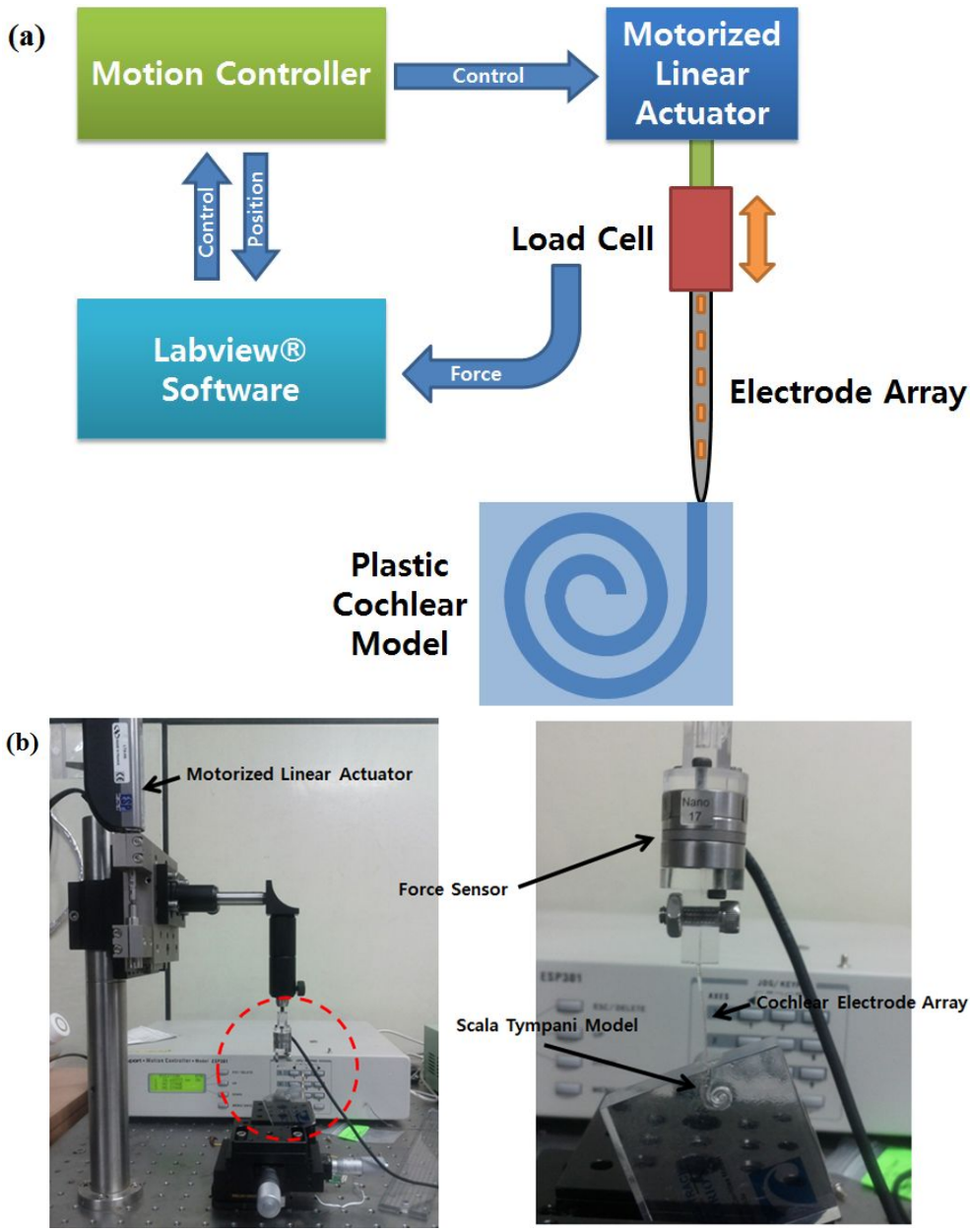

Figure 2.12 Automated Insertion Setup. The load cell (ATI, Nano17, Pinnacle Park Apex, NC, USA) was fixed to the motorized linear actuator (Newport, LTA-HS, Irvine, CA, US). The actuator was controlled by Labview® software, which also recorded the displacement and insertion force. 50% glycerin was used as a lubricant.

2.4.2.3 Human Temporal Bone Insertion Study

Cochlear electrode arrays under development suffer human temporal bone insertion experiment for an assessment of the insertion safety of the electrode arrays [54]. Insertion depth and insertion trauma are evaluated by an investigation of a computed tomography (CT) scan images and an observation of cross-sectioned specimen, respectively. The insertion depth is measured based on the direction of straight basal cochlear duct (figure 2.13).

In the present study, seven temporal bone insertion trials were performed. LCP-based cochlear electrode arrays were inserted into five cochleae. Fresh temporal bones were removed and prepared from donated cadaver specimens within 24 hours of cardiac death. They were then fixed in 10 % formaldehide for 24 hours. All LCP-based cochlear electrode arrays were inserted in standard round window surgical approaches. We prepared a lubricant comprised of 50% glycerin in distilled water and injected it into some specimens. However, there was no difference in insertion depth and trauma between the specimens with and without lubricant. Cochlear electrode insertion trauma was standardized in the following grading scheme: 0, no trauma (figure 2.14); 1, elevation of the basilar membrane (figure 2.15); 2, rupture of the basilar membrane or spiral ligament (figure 2.16); 3, dislocation into the scala vestibuli (figure 2.17); 4, fracture of the osseous spiral lamina or modiolar wall (figure 2.18) [55].

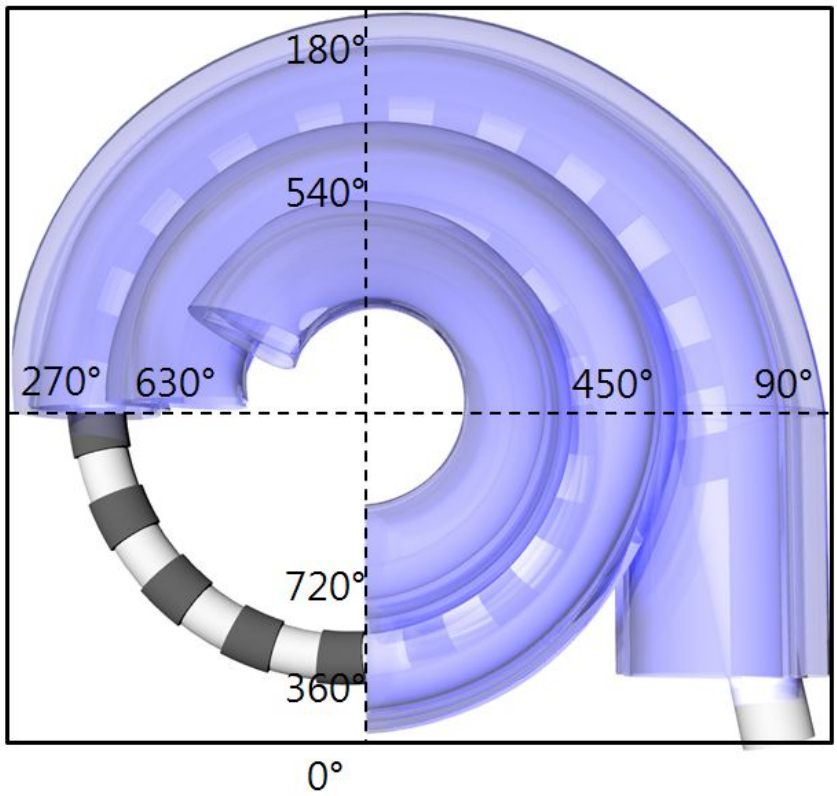

Figure 2.13 Cochlear Angle. The insertion depth was measured based on the direction of straight basal cochlear duct.

Table 2.2 Insertion Trauma.

Grade	Trauma
0	no trauma
1	elevation of the basilar membrane
2	rupture of the basilar membrane or spiral ligament
3	dislocation into the scala vestibule
4	fracture of the osseous spiral lamina or modiolar wall

Figure 2.14 Cochlear Insertion Damage; Grade 0: No Observable Trauma [55].

Figure 2.15 Cochlear Insertion Damage; Grade 1: Elevation of the Basilar Membrane [55].

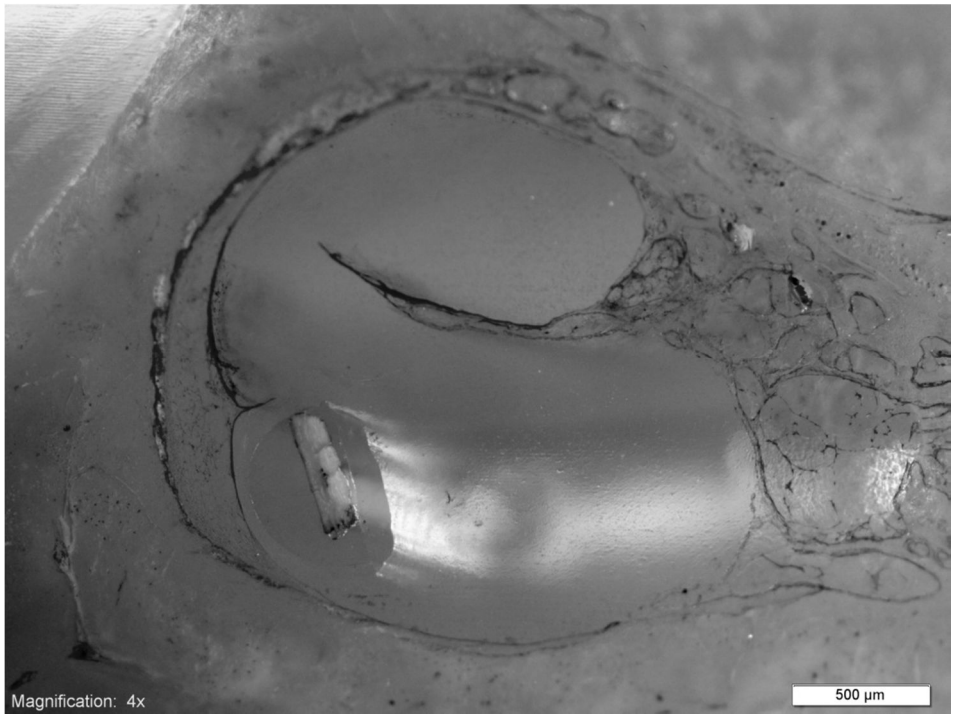

Figure 2.16 Cochlear Insertion Damage; Grade 2: Rupture of Basilar Membrane.

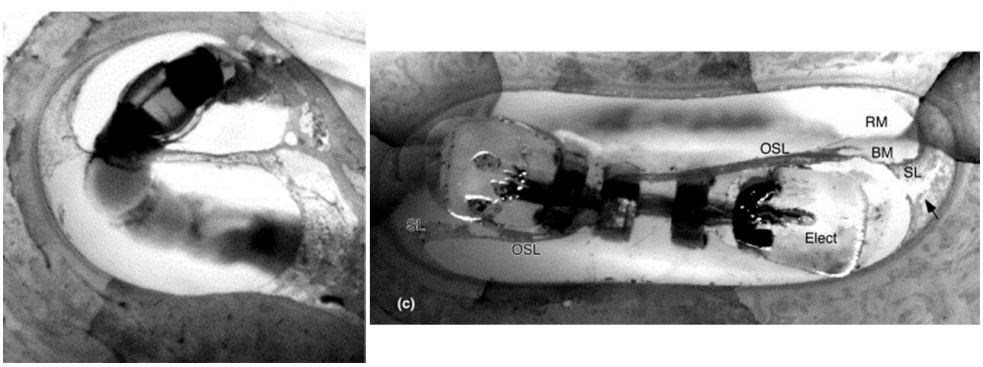

Figure 2.17 Cochlear Insertion Damage; Grade 3: Dislocation into Scala Vestibuli [56].

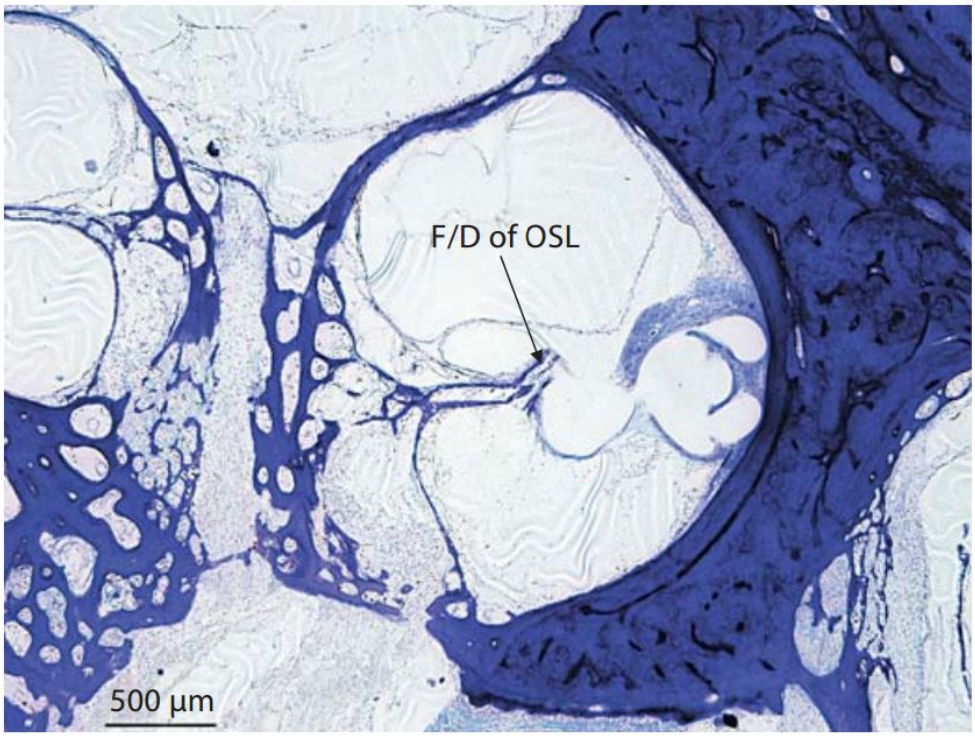

Figure 2.18 Cochlear Insertion Damage; Grade 3: Fracture of the Osseous Spiral Lamina [57].

Chapter III

Results

3.1 Micro-Fabrication Process

The flatness total indicator reading (TIR) values of a bare glass wafer, an LCP-attached wafer using a photoresist adhesion layer and an LCP-attached wafer using a silicone elastomer adhesion layer were 4.8 μm, > 43.7 μm and 16.0 μm, respectively. As shown in figure 3.1 (a), the formation of bubbles led to a non-uniform surface on the LCP film attached by the photoresist layer after 24 hours of the attachment process. On the other hand, the surface of the LCP film attached by the silicone elastomer maintained its flatness without the generation of bubbles. The bumpy surface of the LCP film attached by the photoresist layer showed unmeasurable regions, while the surface of the LCP film attached by the silicone elastomer showed curvature similar to that of the bare wafer.

As shown in figure 3.2 (a), 10 μm × 10 μm square test structures of thick photoresist employed as an electroplating mold were patterned on an LCP substrate with 10 μm spacings. Based on this, fine metal trace wires with cross-sectional dimensions of 10 μm × 5 μm were patterned by means of gold electroplating (figure 3.2 (b)). A multilayered interconnection employing a thermal press bonding process was fabricated without metal trace breakage (figure 3.3 (a)). After the lamination process, the measured alignment error between the substrate and the cover layer was 84.4 ± 12.6 μm. The laser trace burns the LCP film at 82.5 ± 4.2 μm along the trace line. The beam size was 35 μm in diameter. The outlines of the site windows melt and flow inward by 15 ± 2.5 μm (figure 3.3 (c)).

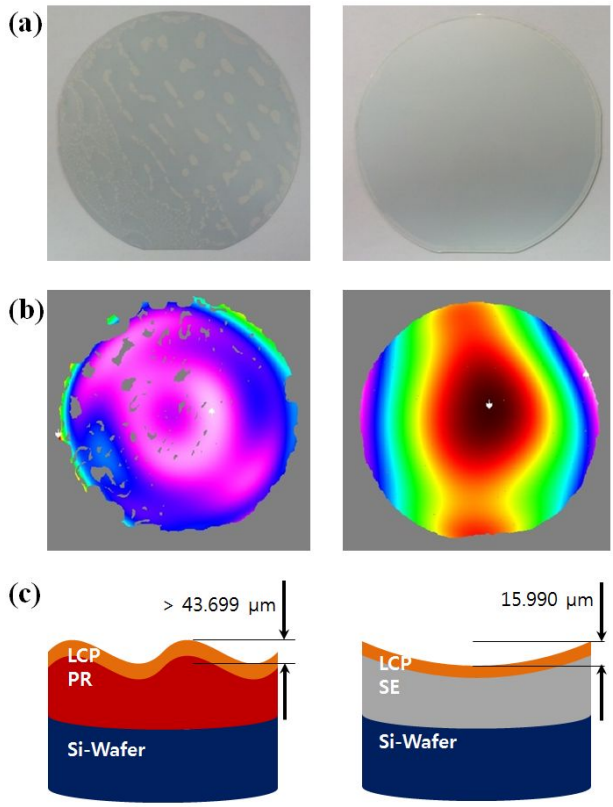

Figure 3.1 Flatness of the LCP Films Attached onto a Silicon Wafer using a Photoresist (left) and a Silicone Elastomer (right): (a) Photographs of the LCP Surfaces after 24 Hours of Attachment: Bubbles generated by the evaporation of solvent on a photoresist formed a bumpy surface. There was no change of the surface of the LCP film attached by the silicone elastomer. (b) Result of the Flatness Measurements: Bumpy surface of the LCP film attached by a photoresist has an unmeasurable region, while the surface of the LCP film attached by silicone elastomer showed curvature similar to that of a bare glass wafer. (c) Flatness TIR Values: The flatness TIR values of the PR-attached and SE-attached samples were > 43.7 μm and 16. 0 μm, respectively. The value of the PR-attached wafer was the result of flatness within a measurable range.

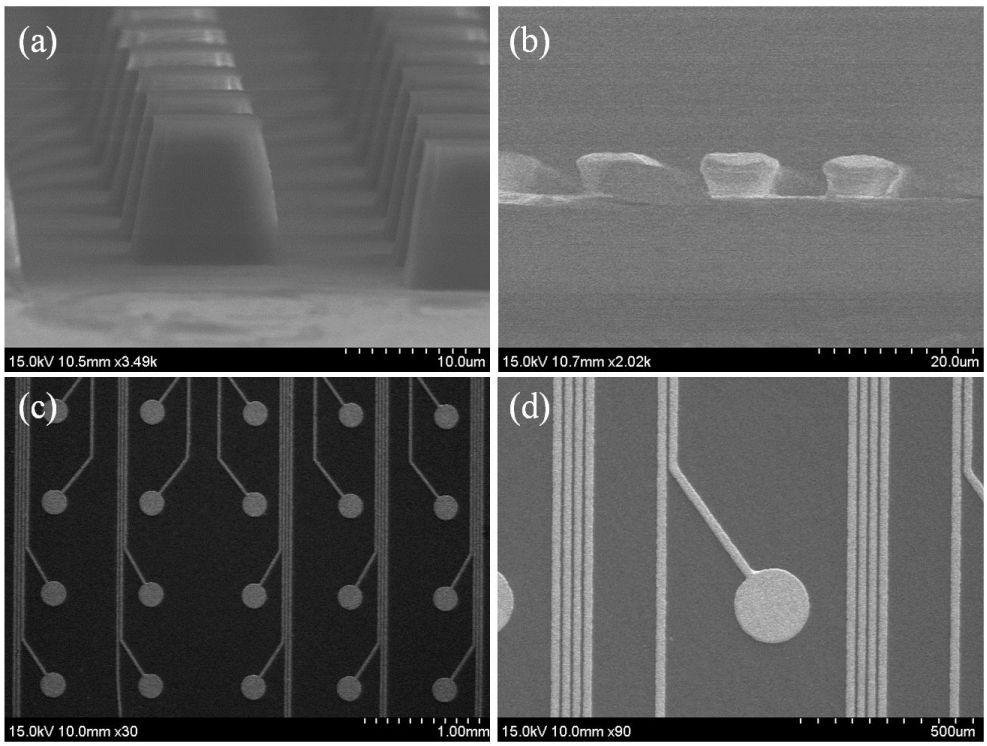

Figure 3.2 Metallization on a LCP Substrate: (a) Photoresist test patterns of 10 μm × 10 μm squares with a 10-μm spacing, (b) cross-section of test patterns after gold electroplating, (c) electrode array patterns, and (d) enlarged image of an electrode site.

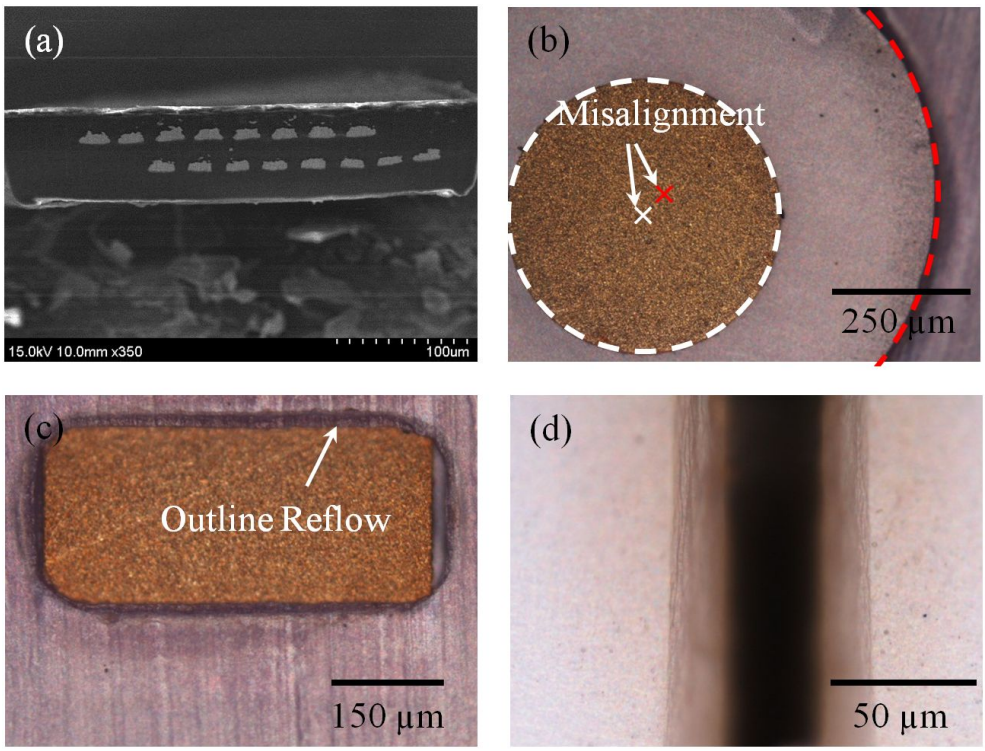

Figure 3.3 Lamination and Laser-Cutting: (a) Cross-section of a multilayered 16-channel interconnection. (b) The measured alignment error between the substrate and the cover layer was 84.4 ± 12.6 µm. (c) Outline of an opening of an electrode site melting and flowing inward by 15 ± 2.5 µm. (d) The width of the laser trace was 82.5 ± 4.2 µm.

3.2 LCP-Based Cochlear Electrode Array

Figure 3.4 (a) describes the shape of the finalized intracochlear electrode array. The photograph of the electrode array shows the iridium oxide stimulation sites molded in silicone elastomer. Though silicone elastomer mold was designed to make a straight carrier, the result showed a gently rounded shape. Through the transparent silicone elastomer, the sawtooth-like LCP leads were observed between the stimulation electrodes. Figure 3.4 (b) shows a cross-sectional view and gives the dimensions of the electrode array. The dimensions of the apex and base were 500 μm × 550 μm and 850 μm × 625 μm, respectively, with a semicircular cross-section. The length of the electrode was 28 mm.

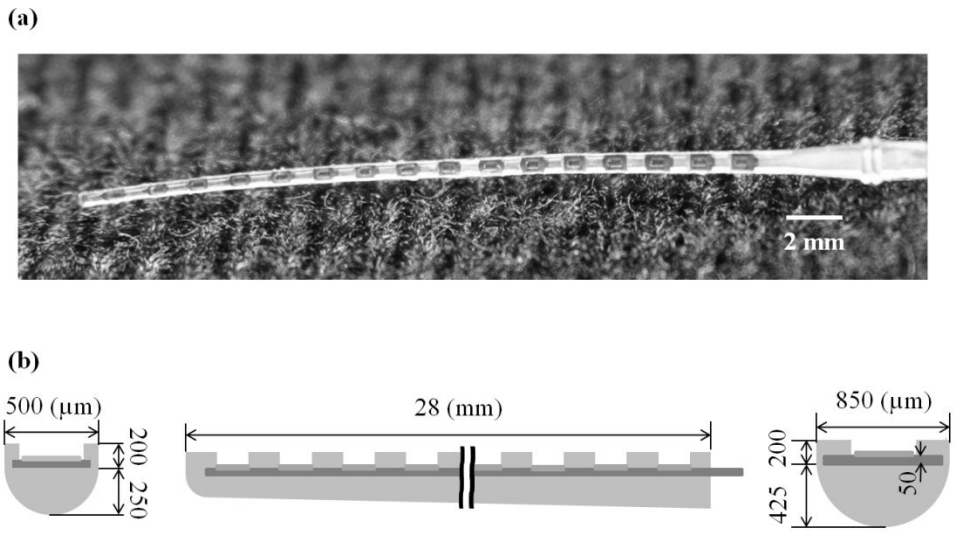

Figure 3.4 Photographs and dimensions of the LCP-based intracochlear microelectrode array. (a) Photograph of the intracochlear electrode array showing the sixteen iridium oxide electrode sites and silicone elastomer windows. Among the electrodes, narrow LCP leads were observed. (b) Cross-sectional views: Apical (left) and basal (right) dissections showed semicircular shape. The areas of cross-section were 500 μm × 550 μm (apex) and 850 μm × 625 μm, respectively. The length of the electrode array was 28 mm (center).

3.3 Electrochemical & Mechanical Property

We observed the charge storage capacity and electrochemical impedance at 1 kHz before and after the iridium oxide electroplating on gold seed layer. Before the electroplating, impedance and charge storage capacity were measured as 564 Ω and 5.6 mC/cm^2, respectively. Likewise, 391 Ω and 38.0 mC/cm^2 were measured after the iridium oxide electroplating. (figure 3.5 and figure 3.6)

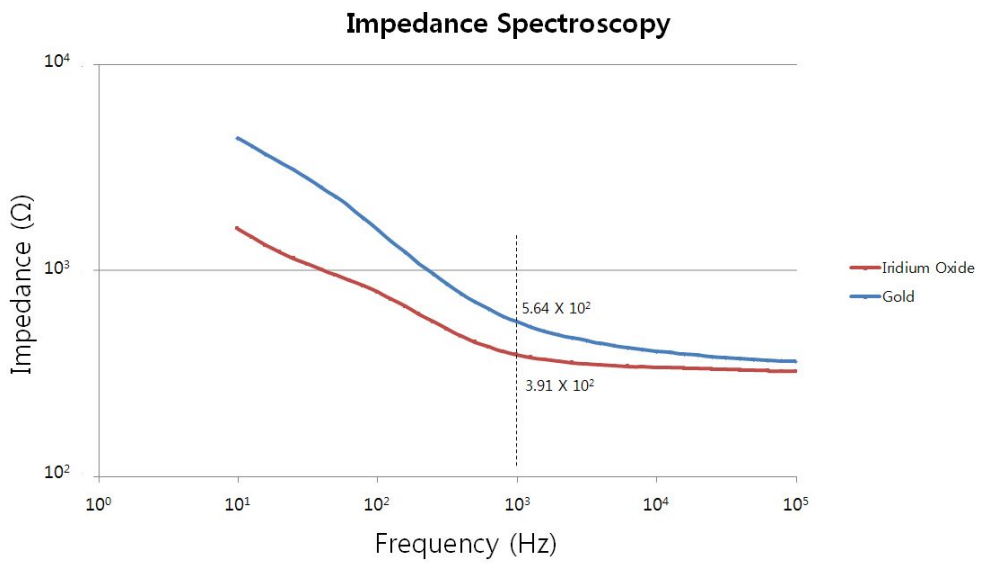

Figure 3.5 Impedance Spectroscopy Result Before and After the Iridium Oxide Electroplating. Before and after the electroplating of iridium oxide, impedances were measured as 564 Ω and 391 Ω, respectively.

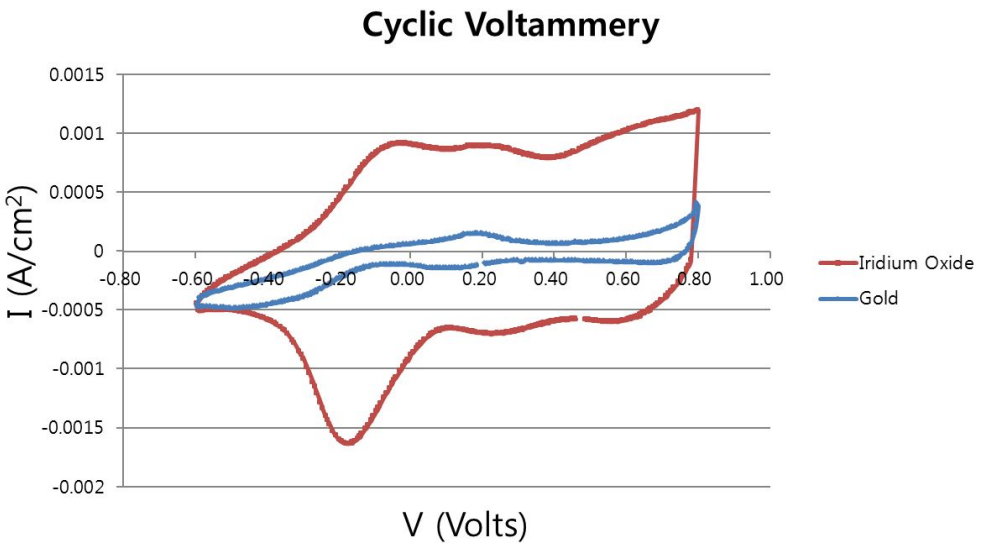

Figure 3.6 Cyclic Voltammetry Result Before and After the Iridium Oxide Electroplating. Before and after the electroplating of iridium oxide, 5.6 mC/cm^2 and 38.0 mC/cm^2 were measured, respectively.

The vertical force and horizontal force of the electrode array were 3.15 g and 1.07 g, respectively. The V/H force ratio was 2.77, which was comparable to that of commercial cochlear electrode arrays [53]. The insertion forces at a displacement of 8 mm from the round window were 17.2 mN (wire-based) and 8.2 mN (LCP-based electrode) (figure 3.7). The LCP-based cochlear electrode array was inserted 3 mm deeper than that of wire-based electrode array. The maximum extraction forces were determined to be 158.5 mN (wire-based) and 110.4 mN (LCP-based electrode) (figure 3.8).

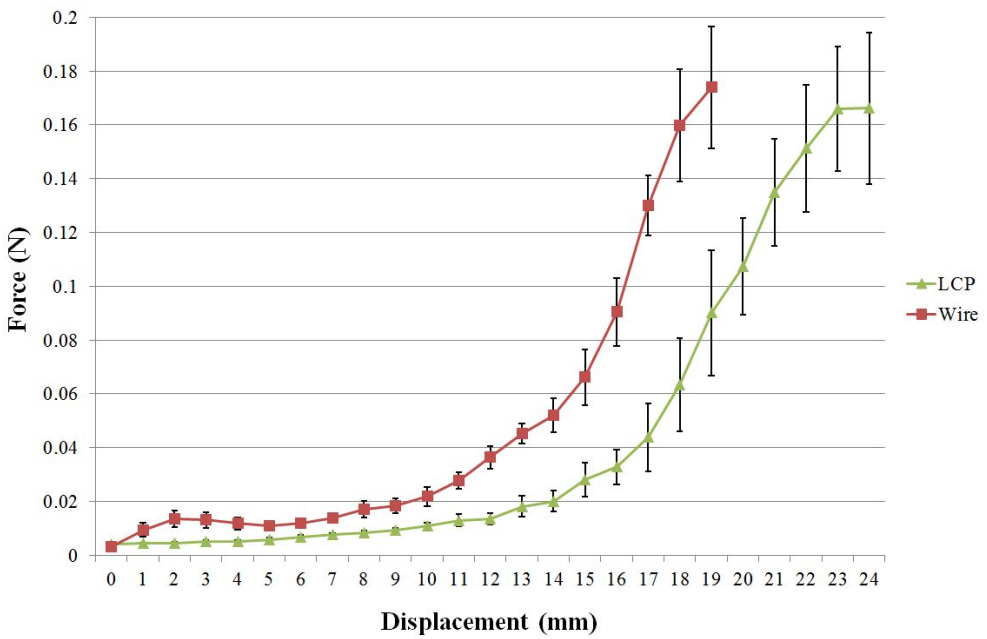

Figure 3.7 Insertion forces of wire-based and LCP-based electrode arrays. The insertion forces at a displacement of 8 mm from the round window were 17.2 mN (wire-based) and 8.2 mN (LCP-based). The final insertion force of the LCP-based electrode was determined to be half that of the wire-based electrode array.

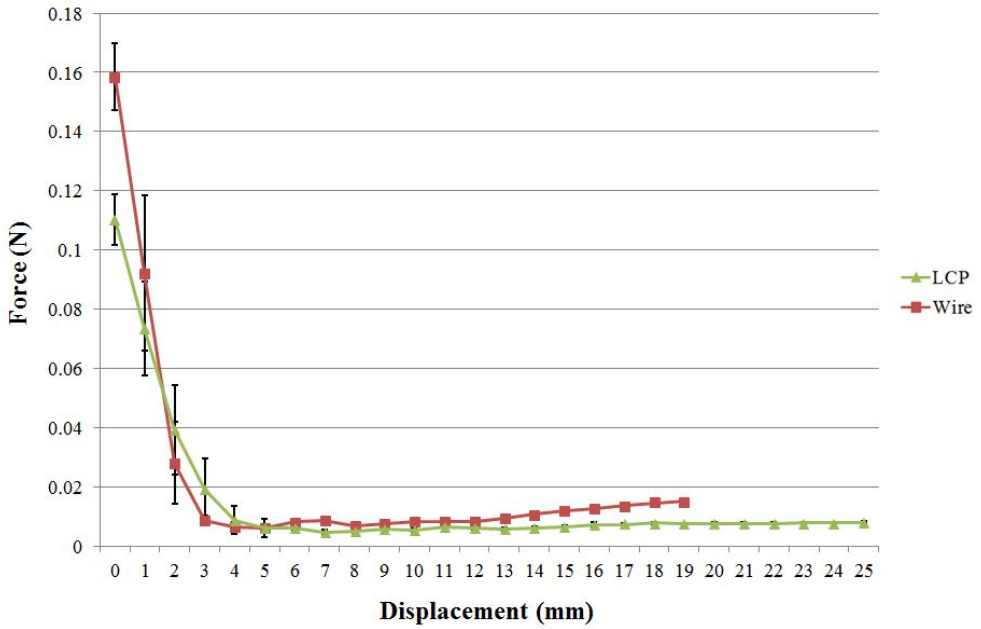

Figure 3.8 Extraction forces of wire-based electrode and LCP electrode arrays. The extraction force of the wire-based straight electrode (158.5 mN) was greater than that of the LCP-based electrode array (110.4 mN).

Table 3.1 Insertion and Extraction Force of Wire-Based and LCP-Based Cochlear Electrode Arrays.

	Wire Based	**LCP Based**
Insertion Force at a Displacement of 8 mm from Round Window	17.2 mN	8.2 mN
Maximum Extraction Force	158.5 mN	110.4 mN

3.4 Human Temporal Bone Insertion Study

The temporal bone study result of LCP-based electrode array was shown in figure 3.10~figure 3.14. As depicted in figure 3.9 the cross-sectioned plane was represented as A-A' and B-B'. The insertion depths of the LCP-based electrode arrays were approximately 405° from round window. Among five cases, two samples were inserted without trauma (grade 0) (figure 3.10 and figure 3.11), while a rupture of the basilar membrane (grade 2) was observed in three cases (figure 3.12, figure. 3.13 and figure. 3.14).

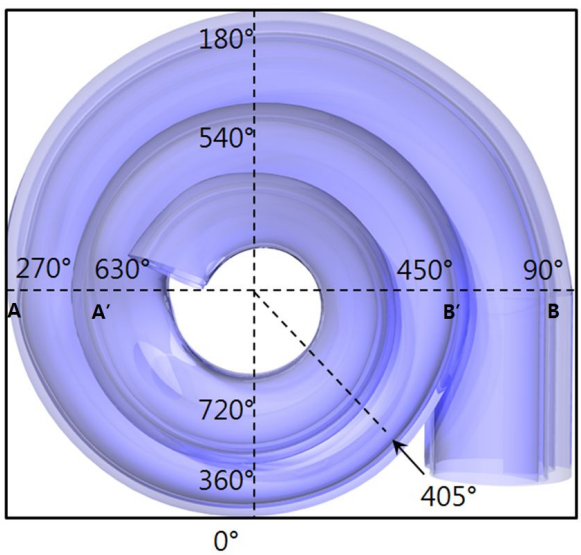

Figure 3.9 Mean Insertion Depth and Cross-Sectioned Plane of Cochleae with LCP-based Cochlear Electrode Arrays. The cross-sectioned plane was represented as A-A' and B-B'. The insertion depths of the LCP-based electrode arrays were approximately 405° from round window.

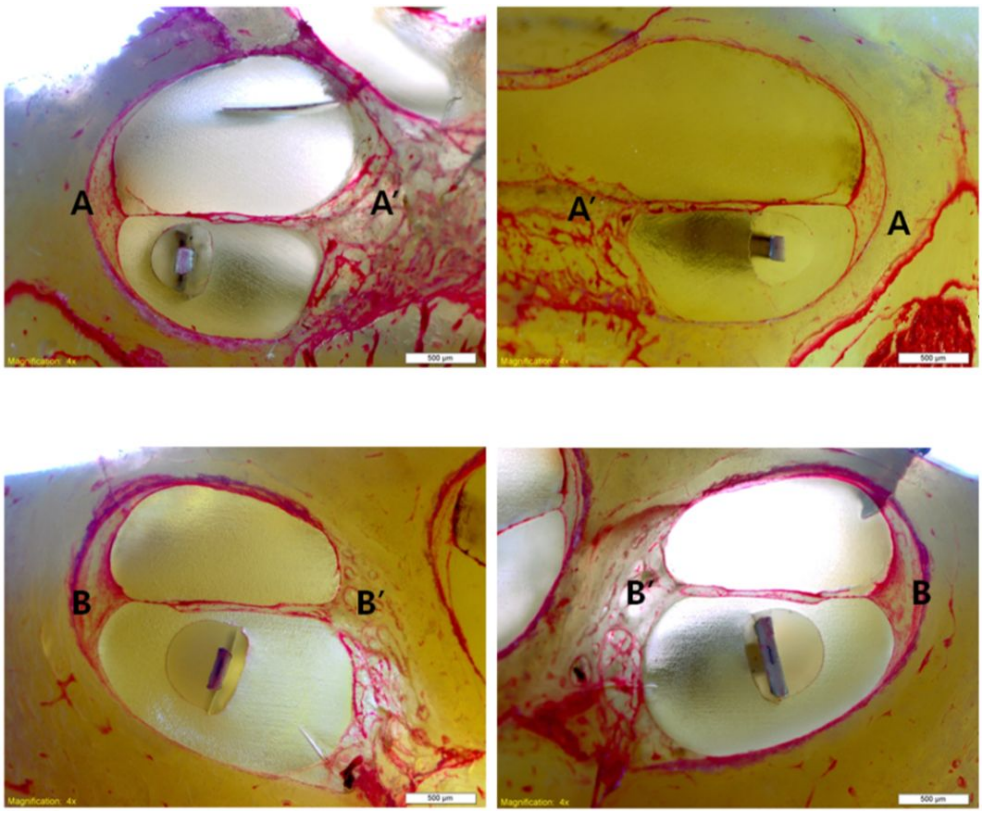

Figure 3.10 Cross-sectional View of the Human Cochlea with LCP-based Cochlear Electrode Array #1, There is no observable trauma.

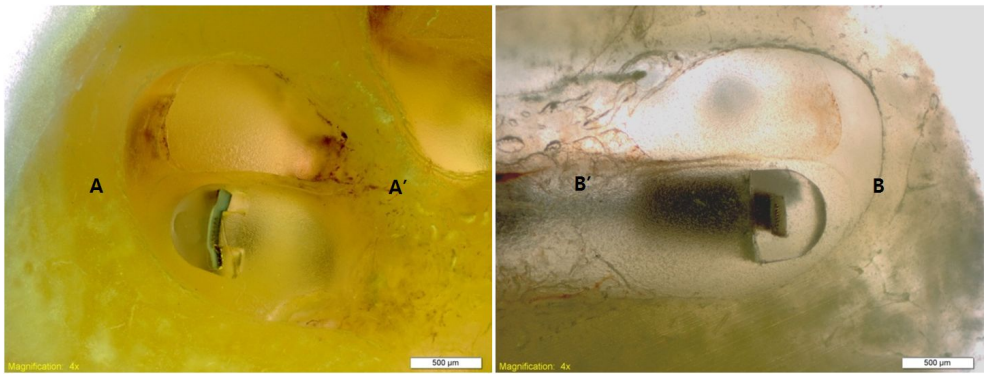

Figure 3.11 Cross-sectional View of the Human Cochlea with LCP-based Cochlear Electrode Array #2, There is no observable trauma.

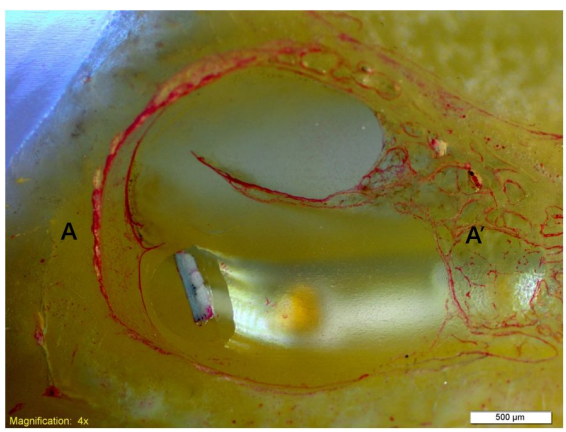

Figure 3.12 Cross-sectional View of the Human Cochlea with LCP-based Cochlear Electrode Array #3, Rupture of the basilar membrane is observed.

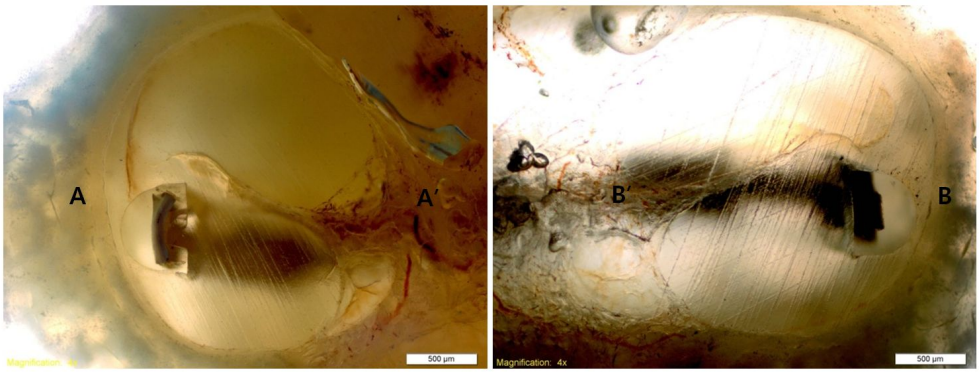

Figure 3.13 Cross-sectional View of the Human Cochlea with LCP-based Cochlear Electrode Array #4, Rupture of the basilar membrane is observed.

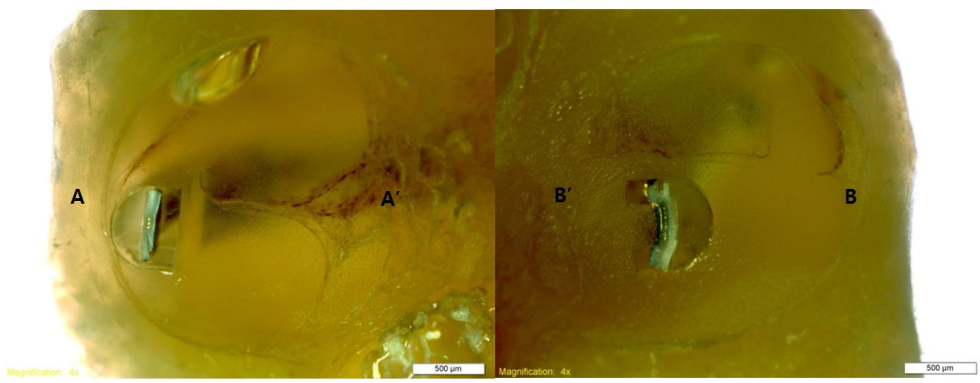

Figure 3.14 Cross-sectional View of the Human Cochlea with LCP-based Cochlear Electrode Array #5, Rupture of the basilar membrane is observed.

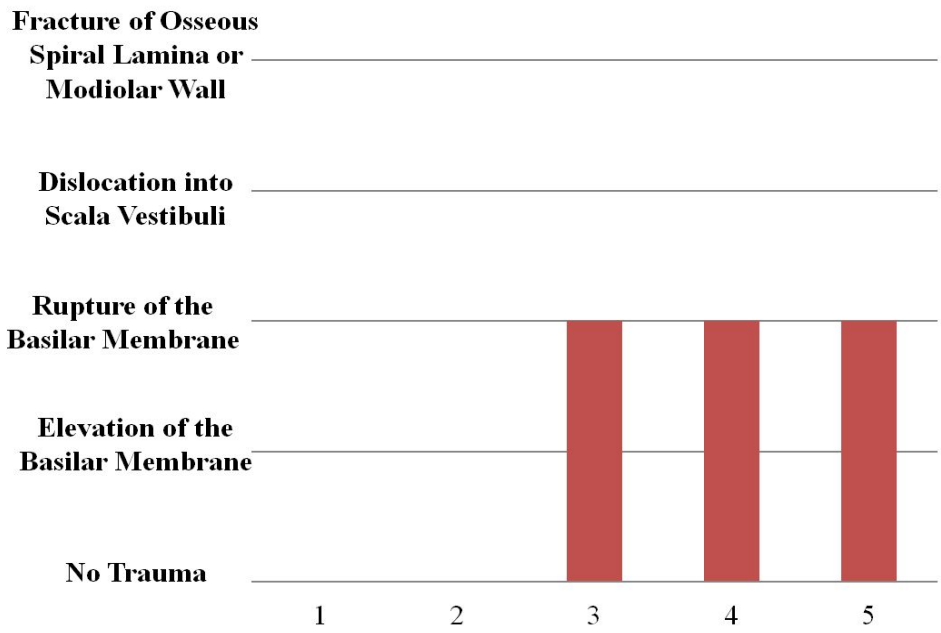

Figure 3.15 Summary of Damage of LCP-Based Intracochlear Electrode Array. Among five cases, two samples were inserted without trauma (grade 0) (figure 3.10 and figure 3.11), while a rupture of the basilar membrane (grade 2) was observed in three cases (figure 3.12, figure. 3.13 and figure. 3.14)

Chapter IV

Discussion

4.1 Micro-Fabrication Process

Conventionally, photoresist layers have been used as adhesion layers for the attachment of LCP films to silicon wafers. However, as shown in figure 3.1, the flatness of the LCP film attached by the photoresist layer here worsens over time due to the bubbles that are generated by the evaporation of the solvent on the photoresist. The evaporation of the solvent on the photoresist adhesion layer becomes more serious in the regular photolithography processes; in other words, soft-baking of the photoresist occurs. The voids made by the solvent vapors are not eliminated after the substrate is cooled to room temperature because the cured photoresist with the solvent vapor is already deformed, losing its adhesion property. On the other hand, no bubbles were found beneath the LCP substrate attached by the silicone elastomer adhesion layer during the baking process.

The flatness also affects resolution of photolithography. The resolution is proportional to the square root of the product of wave length and distance between mask and substrate.

$$Resolution \propto \sqrt{\lambda d}$$

According to the evaluation result of flatness of LCP-attached silicon wafers, the flatness of the LCP-attached wafer using photoresist was approximately 2.7 times greater. In the evaluation, the flatness of a bare glass wafer was measured as 4.8 μm. If a photo-aligner of which minimal resolution is 2.0 μm on bare silicon wafer, the resolution of LCP-attached wafers using silicone elastomer and photo-resist will be 3.7 μm and 6.1 μm, respectively (table 4.1). Moreover, the bubbles induced

between LCP film and photoresist defile surficial uniformity as shown in figure 4.1 (c) while the surface profile of LCP-attached wafer (figure 4.1 (b)) using silicone elastomer showed similar to that of bare glass wafer (figure 4.1 (a)).

Table 4.1 Flatness and Resolution of Photolithography.

Bonding Material	TIR (µm)	Resolution (µm)
Bare Glass Wafer (Control)	**4.8**	**2.0**
Silicone Elastomer	**16.0**	**3.7**
Photoresist	**>43.7**	**> 6.1**

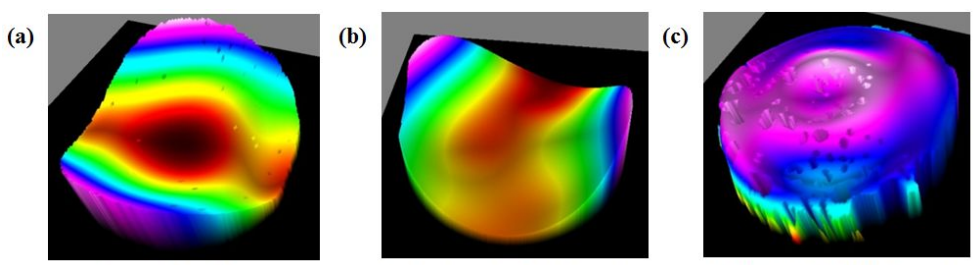

Figure 4.1 Transverse Views of Flatness Measurement of (a) Bare Glass Wafer, (b) LCP-Attached Wafer using Silicone Elastomer and (c) LCP-Attached Wafer using Photoresist.

The detachment of the LCP films should be considered during the micro-patterning process. Because the photoresist adhesion layer dissolves in the photoresist developer, the LCP film should adhere onto the wafer again for further processes. Moreover, if dissoluble microstructures are patterned on the film, e.g., a photoresist electroplating mold, a photoresist adhesion layer cannot be used because the solvent for the detachment of the LCP film also dissolves the microstructure patterned onto the LCP film. The elastomer adhesion layer suggested in this study can preserve dissolvable structures in a photoresist-dissolving solution. However, while the photoresist-adhered film is detached by dissolving the photoresist layer in a solvent, the silicone elastomer-adhered film is not detached unless mechanical peeling stress is applied to it. Thus, an elastomer-attached LCP film can be employed in further micro-fabrication processes even if it is immersed in a photoresist-dissolvable solution. Because the bonding strength between the silicone elastomer and the LCP film is the van der Waals force [58, 59], the bonding is reversible, which means that the elastomer-coated silicon wafer can be reused for another LCP film.

Table 4.2 Comparison of Bonding Methods

Wafer-LCP Bonding	Reversibility	Line Pitch	Detachment
Photoresist	×	8 μm	Dissolve the PR
		20 μm	
Silicone Elastomer	o	**<10 μm**	**Peeling Off**
		20 μm	

The minimum line width which can be patterned on the LCP substrate was 2~3μm on a thin film metal layer with a thickness of less than 300 nm. However, these dimensions were rarely utilized in the LCP thermal bonding process because the line traces were easily broken by high temperatures and pressures. In this study, relatively thick 10-μm-wide line traces were utilized for a reproducible process. The major factor which affects the process tolerance was lamination-alignment error. As shown in figure 4.2 (a), The width of the LCP structure in the LCP-based cochlear electrode array (W_T) was determined by the width of the electrode (W_S), the number of channels ($N_{channel}$), the minimal line pitch (P), the error in the laser machining (electrode site: E_S, outline: E_O) and number of LCP layers where the channel was patterned (N_{layer}). In this study, LCP-based microelectrode arrays employed a design scheme which arranges stimulation sites at the center and lead wires around the stimulation sites [17]. Then, a pre-laser-cut cover layer with site opening windows was laminated on the metal-patterned substrate. The spacing between the site electrode and lead wire was larger than the lamination alignment

error so that the lead wire was not exposed through the pre-laser-cut site openings of the cover layer. The electrode site was also larger than the opening windows of the cover to the extent of the lamination alignment error. However, the final laser-cutting process had to be precisely controlled so as not to cut the lead wires on the outer-most trace in case a narrow electrode array was used. The LCP structure introduced in this study consisted of a single patterned LCP layer; i.e., all of the lead wires were patterned on the same surface. In this case, the width is expressed by the following equation:

$$W_T = W_S + P \times N_{channel} + 2(E_S + E_O),$$

$$\text{where } P = 0 \text{ and } E_O = 0 \text{ if } N_{channel} = 1.$$

As number of channels increases, the width of the LCP film needed for the electrode and the lead wire also increases in proportion to the line pitch (figure 4.2 (b)). The width of the LCP-based electrode array, which has 0.3-mm-wide electrode sites, spans from 0.5 mm (tip) to 1.02 mm (base) if E_S and E_O are 0.1 mm and P is 20 μm.

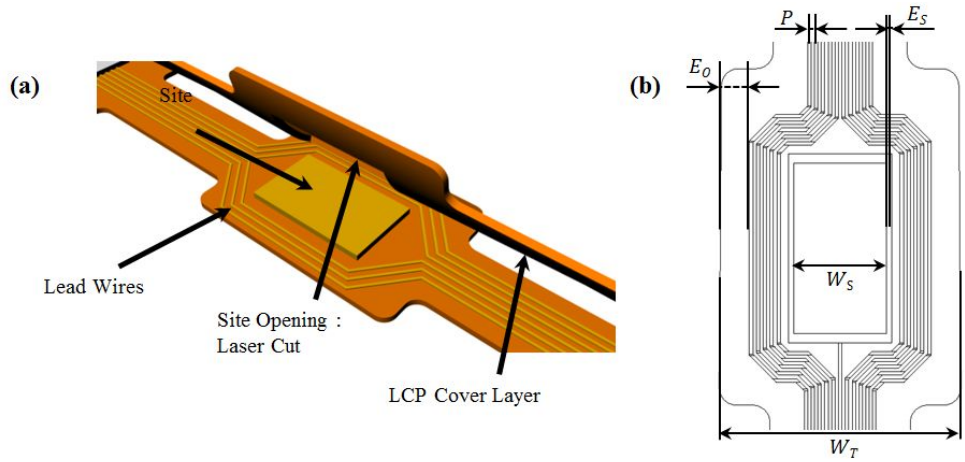

Figure 4.2 Structure and Dimensions of the LCP Electrode Array (a) Structure: In this study, LCP-based microelectrode arrays employed a design scheme which arranges stimulation sites at the center and lead wires around the stimulation sites. Then, a pre-laser-cut cover layer with site opening windows is laminated on the metal-patterned substrate. (b) Dimensions of LCP Electrode Array: The electrode site is positioned at the center of the lead wires. The spacing between the electrode site and the inner wires should be larger than the lamination alignment error. Outermost lead wires are easily cut by a laser.

4.2 Comparison of LCP-Based Intracochlear Electrode Array to Conventional Intracochlear Electrode Arrays

Conventional intracochlear electrode arrays employ platinum-iridium wires as a reinforcement material. In table 4.3, properties of currently most popular intracochlear electrode arrays and the LCP-based electrode array were specified. The Nucleus® 422 electrode is the industry's thinnest electrode array of which apical diameter is 0.3 mm. On the other hand, the apical dimension of the MED-EL Flexsoft™ electrode array is 0.5×0.4 mm^2. However, stiffness of an intracochlear electrode array is not determined by the dimensions of silicone elastomer carrier but by the reinforcement structure in to carrier. Both Nucleus® CI 422 and Flexsoft™ are uses platinum-iridium alloy as their lead wires which become reinforcement. While Nucleus® CI 422 employs straight platinum-iridium wires, Flexsoft™ utilizes wave-shaped wires for reduction of rigidity [60]. On the other hand, the stiffness of the LCP-based intracochlear electrode array is determined by LCP structure. Before molding, the LCP-based cochlear electrode array had straight shape which as not flexible as much as wave-shape structure as insisted in wire-based electrode arrays. However, the LCP-based electrode array was mildly pressed in stepwise molding process, which might vary the mechanical property of straight LCP structure. The mechanical property of the LCP-based electrode will be further discussed in section 4.3.

The electrode sites of both conventional electrode arrays are fabricated by similar manner described in figure 2.10. Therefore, the surfaces of electrode sites

are located in same surface of silicone elastomer carrier. However, the electrode sites of the LCP-based intracochlear electrode are recessed by 200 μm. This profile may influence the distribution of electrical current. This is discussed in section 4.4.

Table 4.3 Comparison of Intracochlear Electrode Arrays

	Cochlear™ Nucleus® CI422	**MED-EL FLEXSOFT™**	**LCP-Based CI Electrode**
Dimension-Tip (mm^2)	0.3 × 0.3 (Circular)	0.5 × 0.4 (Oval)	0.5 × 0.45
Dimension-Base (mm^2)	0.6 ×0.6 (Circular)	1.3 × 1.3 (Circular)	0.85 × 0.625 (Semi-Circular)
Active Length (mm)	20	26.4	26.5
Number of Sites (EA)	22	19 (5 single, 14 pair)	16
Reinforcement	Straight Pt/Ir Wires	Wavy Pt/Ir Wires	LCP (Wavy)
Electrode Shape	Half-Banded Surface	Oval	Rectangle (Recessed)

4.3 Mechanical Property of Cochlear Electrode Array

The manufacturing process of the conventional cochlear electrode arrays consists of the forming of electrode sites, the welding of each electrode to a lead wire, fixation of the electrode to a mold, and injection molding. Most of the processes are manually done under a stereoscopic microscope to make a 12- to 22-channel electrode array. However, 208 electrode sites and lead wires on 13 electrode arrays were easily patterned at once on an LCP-coated silicon wafer by photolithography. The metal-patterned LCP films were encapsulated by a thermal press bonding process followed by an automated laser machining process. In contrast to the conventional molding process which fixes each electrode to an aligned position on a mold one by one, the proposed self-aligning injection molding process used a micro-machined structure of an LCP-based electrode array for alignment and fixation. Because the LCP-based electrode array was inserted into a preformed silicone structure, each electrode site fixed itself at aligned position. The proposed automated manufacturing process can lower the number of fabrication errors and increase productivity, resulting in a low-cost cochlear implant system. These aspects will contribute to an increase in the number of potential cochlear implant recipients even in developing or underdeveloped countries.

The wire-based comparator electrode was tested by Rebscher et al. in 2008 [53]. According to their article, the electrode showed 0 % of trauma while Cochlear Banded™ and Cochlear Contour™ showed rates of 37.5 % and 38.9 %,

respectively. The insertion force data were not produced in the study. However, the mean stiffness was 0.8 g, while these values of the Cochlear Banded™ and Cochlear Contour™ types were 0.6 g and 1.65 g, respectively. Because the insertion trauma is related not only to the insertion force but also to the insertion depth and dimension of electrode array, whether the stiffness has a negative relationship with the insertion trauma is unclear. Nevertheless, the mechanical properties of the cochlear electrode array are still closely related to the degree of insertion safety. Several current major cochlear implant manufacturers, including Cochlear Ltd., Med-El, and Advanced Bionics, have developed electrode arrays which have low levels of insertion force, providing evidence of atraumatic insertion [61]. There are two types of electrode arrays, those with a straight electrode and those with a perimodiolar electrode with a stylet. The straight electrode array is inserted into the cochlear along the outer wall of the scala tympani. The initial insertion force is measured at the moment the apical electrode array tip hits the outer wall of the scala tympani and increases as the number of wires contained in the carrier increases. On the other hand, the stiffness of the LCP-based electrode array is determined by the thickness of the LCP film. In this study, eight to sixteen electrode array channels are patterned on a single layer of LCP film, which means that the difference in the stiffness between the base and the apex is not as much as that in the wire-based electrode array, as shown in figure 3.7.

The extraction damage should be considered because four to six re-implantations can be expected with very young recipients throughout their lifetimes [62]. The plastic deformation of the straight wire-based electrode is one of the

sources of the extraction force. Moreover, a perimodiolar electrode requires extra force to uncoil the pre-shaped carrier. Because LCP is an elastic material, the LCP-based electrode tends to maintain its original shape. Thus, the extraction force of the LCP-based electrode is less than that of the wire-based electrode array, as shown in figure 3.8. The LCP-based electrode has less insertion and extraction force than conventional wire-based electrode arrays.

The LCP electrode array encapsulated by silicone elastomer had wavy shape because the electrode site regions were pushed by cover mold during secondary molding as depicted in figure 4.3. The mechanical property of the wavy structure may be different from straight LCP-based electrode array. To investigate the differences of mechanical properties of straight structure and wavy structure, simple modeling was performed as depicted in figure 4.4.

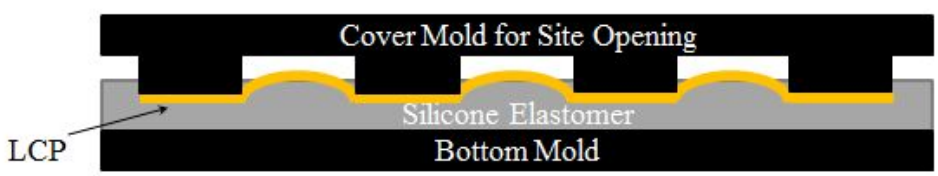

Figure 4.3 Secondary Molding for Encapsulation and Site Opening of LCP-Based Electrode Array. The LCP electrode array encapsulated by silicone elastomer has wavy shape because the electrode site regions were pushed by cover mold during secondary molding.

Figure 4.4 describes two structures as long as interval of adjacent electrodes of LCP-based electrode array. The width and the height were 0.2 mm and 50 μm, respectively. Figure 4.4 (a) represents straight LCP-based electrode array. Likewise, figure 4.4 (b) represents the aforementioned wavy structure of LCP-based electrode array after molding process for encapsulation and site opening. In a simulation software (ANSYS® 14 Workbench, ANSYS, Inc., Canonsburg, PA, US), the terminal of each structure was bent as much as 0.5 mm from its original shape. These models were bent orthogonal axes, axis of width (figure 4.5 (a, b)) and axis of height (figure 4.5 (c, d)).

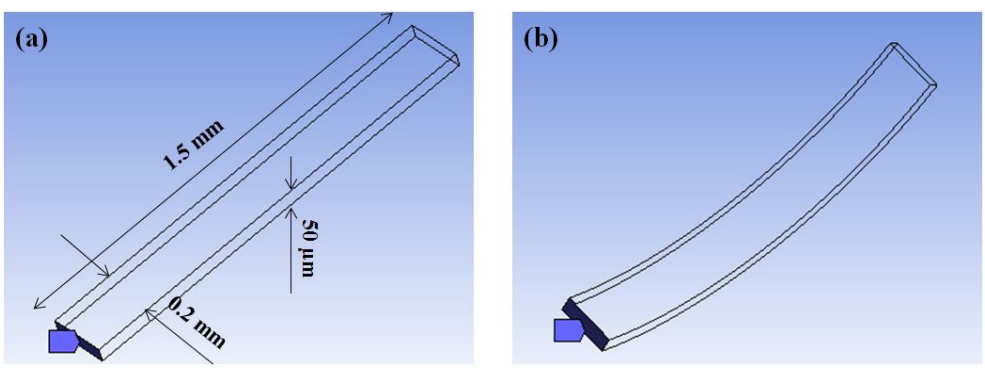

Figure 4.4 Two Structures Represent Different LCP Structure. (a) Straight LCP-based electrode array. (b) Wavy structure of LCP-based electrode array after molding process for encapsulation and site opening.

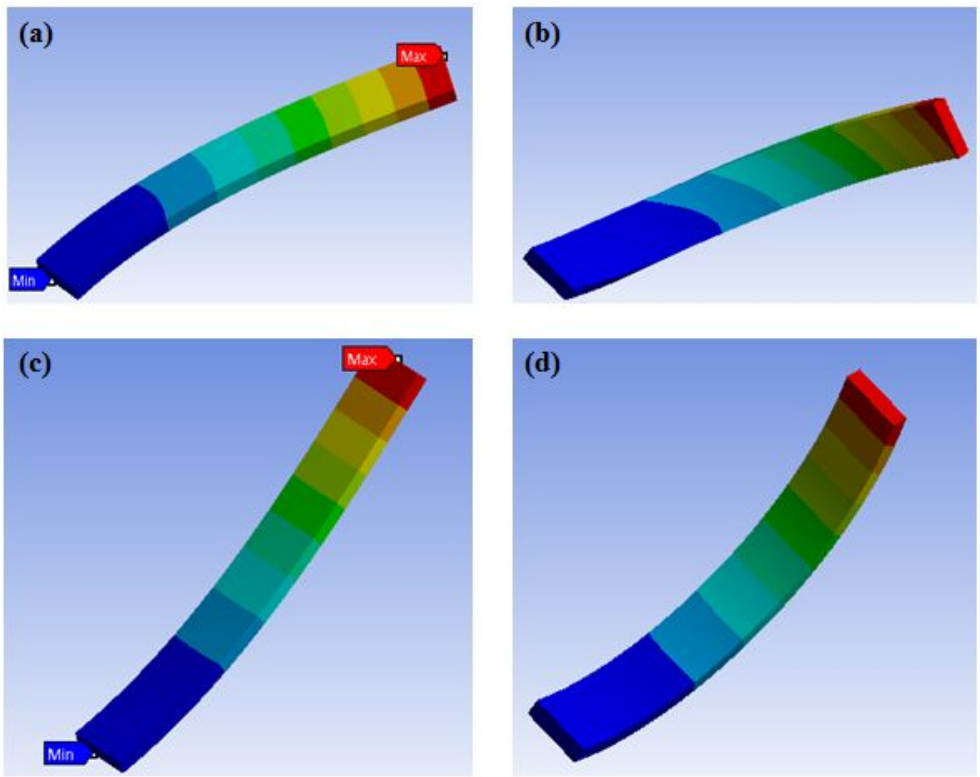

Figure 4.5 Deformation of LCP Models. (a) Straight LCP Bent along the Direction of Width. (b) Wavy LCP Bent along the Direction of Width. (c) Straight LCP Bent along the Direction of Height. (d) Wavy LCP Bent Along the Direction of Height. Each Model was bent as much as 0.5 mm from its original shape.

The maximal reaction force of straight LCP structure bent along the direction of width was 16.74 mN while the reaction force of the wavy model was 4.21 mN. Likewise, the maximal reaction force of straight LCP structure bent along the direction of height was 1.23 mN, while the reaction force of the wavy model was 1.32 mN. As described in figure 4.6, the direction of height and direction of width are orthogonal and parallel to the modiolus, respectively. Since the suggested LCP-based Intracochlear electrode array is not peri-modiolar, but is straight, the

electrode array propagates along the lateral wall of the cochlea. The cochlea has helical structure, which means the intracochlear electrode array should bent along not only toward modiolus but also toward apex of the cochlea. In the case of straight LCP structure, the ratio of vertical force and horizontal force ($F_{V/H}$) is 13.6. On the other hand, the $F_{V/H}$ of wavy LCP structure is 3.2. Interestingly, the $F_{V/H}$ of wavy LCP structure is similar to that of measured $F_{V/H}$ in the section 3.3. This asymmetry of reaction forces may helpful for insertion of film-based intracochlear electrode array. However, excessive vertical force may impede the propagation of intracochlear electrode array because the electrode array should be bent more toward apex as the electrode array is inserted into deeper region. In spite of minor increment of horizontal force of wavy LCP structure, the vertical force reduced dramatically results in a desirable mechanical property.

Table 4.4 Simulation Result of Reaction Forces

	Horizontal Force (Direction of Height)	**Vertical Force (Direction of Width)**	**$F_{V/H}$**
Straight LCP	1.23 mN	16.74 mN	13.6
Wavy LCP	1.32 mN	4.21 mN	3.2

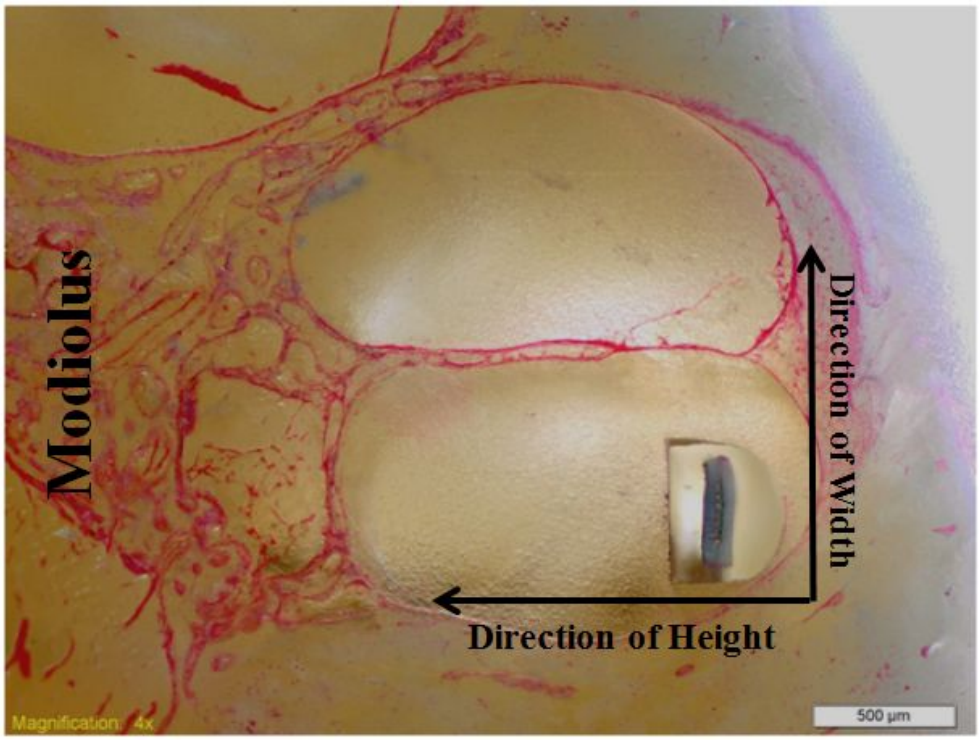

Figure 4.6 Cross-Sectional View of Cochlea with LCP-Based Intracochlear Electrode Array. Excessive vertical force may impede the propagation of intracochlear electrode array because the electrode array should be bent more toward apex as the electrode array is inserted into deeper region.

4.4 Silicone Encapsulation

The LCP material is a very strong and stable material when it is used for semiconductor packaging applications or in electronic components. As a film, it becomes flexible along its normal direction, but the mechanical properties of LCP are still stiff along its tangential direction. Thus, sharp edges of neural electrodes based on a rigid film substrate may be traumatic to the surrounding tissue. To protect the surrounding tissue against the edges of film-based neural electrode arrays, encapsulation of the electrode array must be employed. There are various types of silicone rubber with mechanical properties similar to that of the surrounding tissue implanted in bodies. However, without considering the electrode site openings, it is difficult to open electrode sites which are buried in silicone rubber. In this case, a polymer ablation process such as laser ablation or dry etching can be applied. However, the laser ablation process can burn the elastomer and electrode, and dry-etching is time-consuming. In our work, a micro-molding process without an ablation process was exploited. Self-aligning during the elastomer molding process could precisely locate the electrode array on the opening structure of the upper mold and successfully opened the electrode sites.

The recessed structure may influence the distribution of electrical current. To estimate the difference between recessed structure and non-recessed structure, 2-D simulation was performed in COMSOL Multiphysics (COMSOL Multi-Physics, COMSOL Inc, Burlington, MA, US). Two different electrode profiles were modeled and electrical current of 100 $\mu A/mm^2$ was applied to each electrode

contacts. As shown in figure 4.7, the current flux of recessed structure was guided along the wall of silicone elastomer while the current flux of planar structure formed radial shape. This result may suggest the guidance of stimulation current. As shown in figure 4.7 (a), the recessed can deliver the electrical current in the normal direction of electrode surface. Conventionally, virtual channel have been suggested to overcome limited number of electrode sites. However, through the suggested micro-fabrication process, the micro-sized ultra-fine electrode sites can be fabricated in finer structure of LCP. Thus, without virtual channel scheme, the electrical stimulation can be delivered to more minute area.

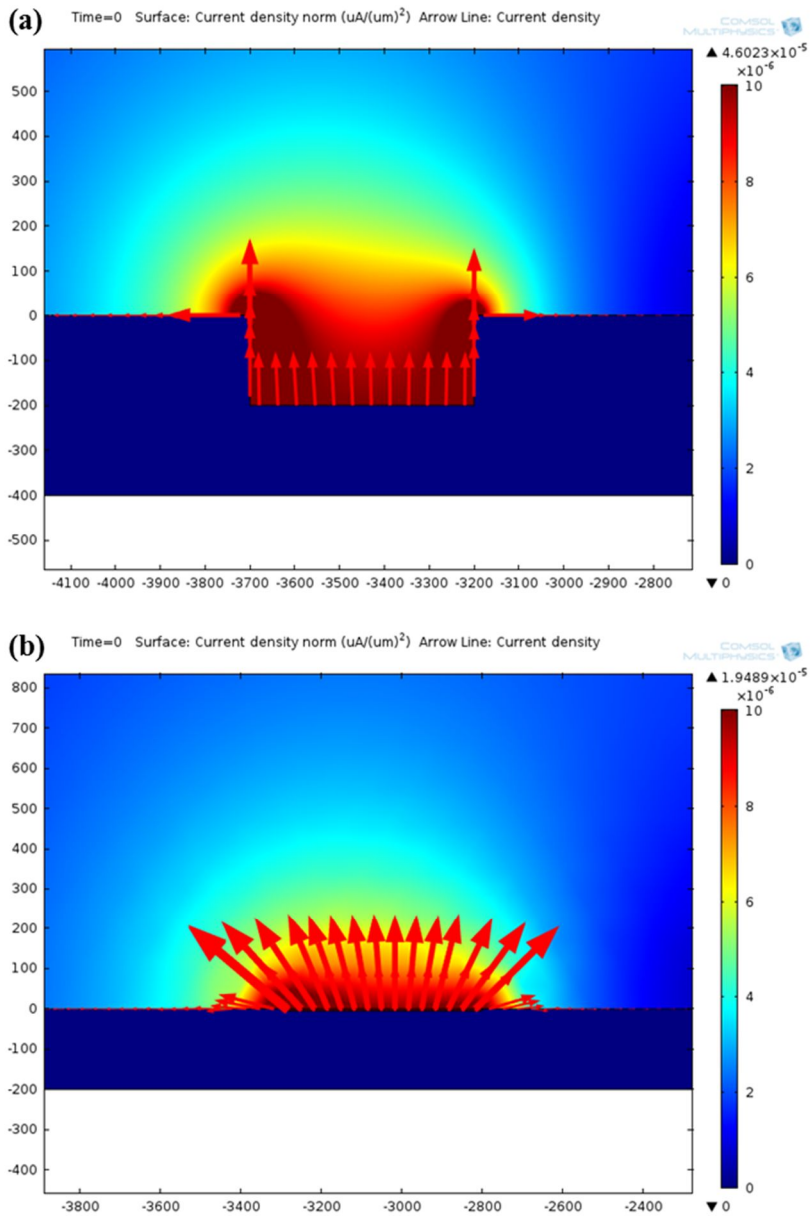

Figure 4.7 Current Distribution According to the Structure of Electrode Sites. (a) Recessed Structure: The current flux of recessed structure was guided along the wall of silicone elastomer. (b) Non-Recessed Structure: The current flux of planar structure formed radial shape.

4.5 Insertion Safety and Insertion Depth

From human temporal bone insertion study, we obtained two results without trauma. And another three electrode arrays were inserted with rupture of basilar membrane. To compare this result to conventional intracochlear electrode array, we plotted a histogram based on a report which evaluated commercially available intracochlear electrode arrays from three leading companies, Cochlear Ltd., MED-EL and Advanced Bionics corp. [55]. The report evaluated three peirmodiolar electrode arrays, Contour™ (Cochlear Ltd.), HiFocusII™ (Advanced Bionics corp.) and Comni40+ PM™ (MED-EL). Five trials of human temporal bone study were performed for each electrode array. As shown in table 4.5, Contour™ inserted with no trauma in three trials while two results showed fracture of osseous spiral lamina, highest grade of trauma criteria. HiFocusII™ and Combi40+ PM™ showed relatively even distribution over all criteria.

Table 4.5 Insertion Damage of Three Perimodiolar Electrode Arrays (Data From [55])

Electrode Array	Grade 0	Grade 1	Grade 2	Grade 3	Grade 4
Contour™	3	-	-	-	2
HiFocusII™	1	2	1	1	-
Combi40+ PM™	2	1	1	-	1

In figure 4.8, human temporal bone insertion study results of LCP-based intracochlear electrode arrays are shown in a histogram with aforementioned commercial electrode arrays. The human temporal bone insertion results of LCP-based electrode array have not shown any major trauma while other three electrode arrays inserted with major trauma high than grade 2 in a few trials. Though the comparison between suggested LCP-based straight electrode array to the perimodiolar electrode arrays do not seem appropriate, it is meaningful that the LCP-based intracochlear electrode array showed comparable result to the commercially available intracochlear electrode arrays.

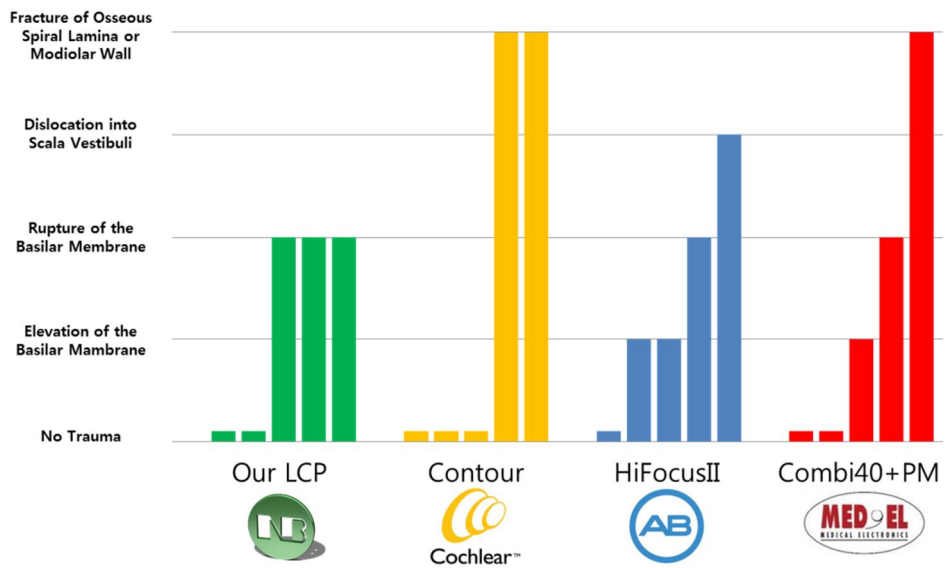

Figure 4.8 Insertion Trauma. Comparison with Current Manufacturers [55].

The total length of the suggested LCP-based intracochlear electrode array is 28 mm. In consideration of its length, the suggested intracochlear electrode array should have been reached more than 600°. However, the mean insertion depth was 405°. Cochlea analyses sound spectrum using its helical duct structure which has narrower apical region. The distance from stapes to the place of maximum displacement was reported in [63] (figure 4.9) and it was expressed by following equation in case of human.

$$F = A(10^{ax} - k)$$

$$A = 165$$

$$a = 0.06$$

$$k = 1$$

Because intact human cochlea processes 20 Hz to 20 kHz, insertion depth as deep as 405° of LCP-based cochlear electrode array may not provide sound information with low frequency. Current cochlear implant devices provide sounds with lower frequency than the Greenwood center frequency at the place where their electrode tip is [64, 65]. Moreover it was reported that the deeper electrode insertion is associated with improved postoperative speech perception [66]. Deeply inserted electrode site may be matched closer with the place-equivalent acoustic pitches, results in better performance. The Greenwood frequency at the tip of suggested LCP-based electrode array is 700 Hz, approximately (figure 4.10). The reason of incomplete insertion may be as follows.

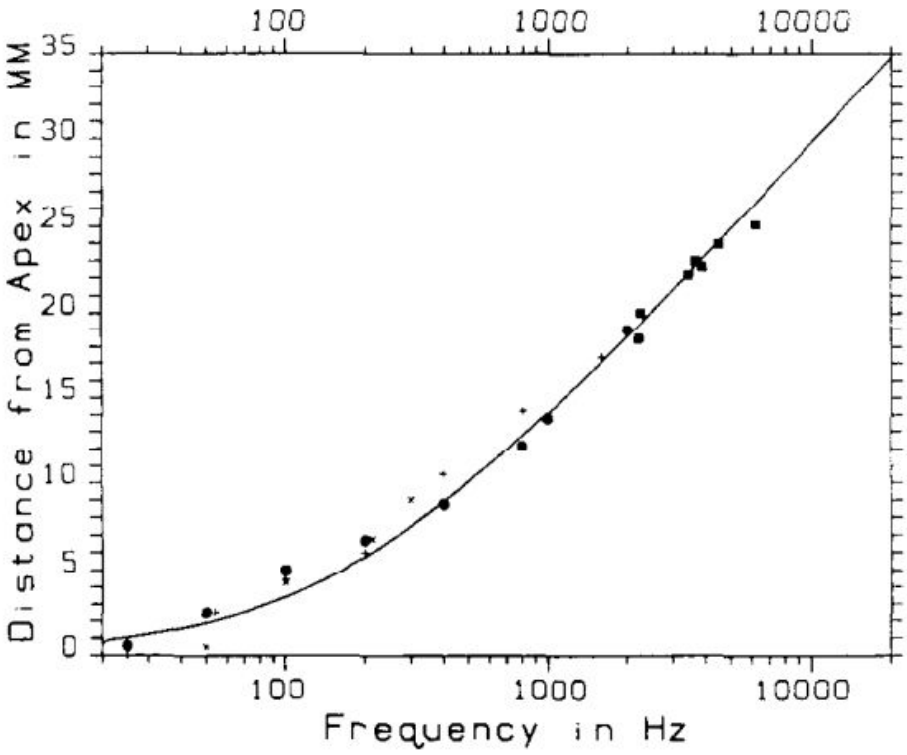

Figure 4.9 Distance from Stapes to the Place of Maximum Displacement, as a Function of Frequency [63].

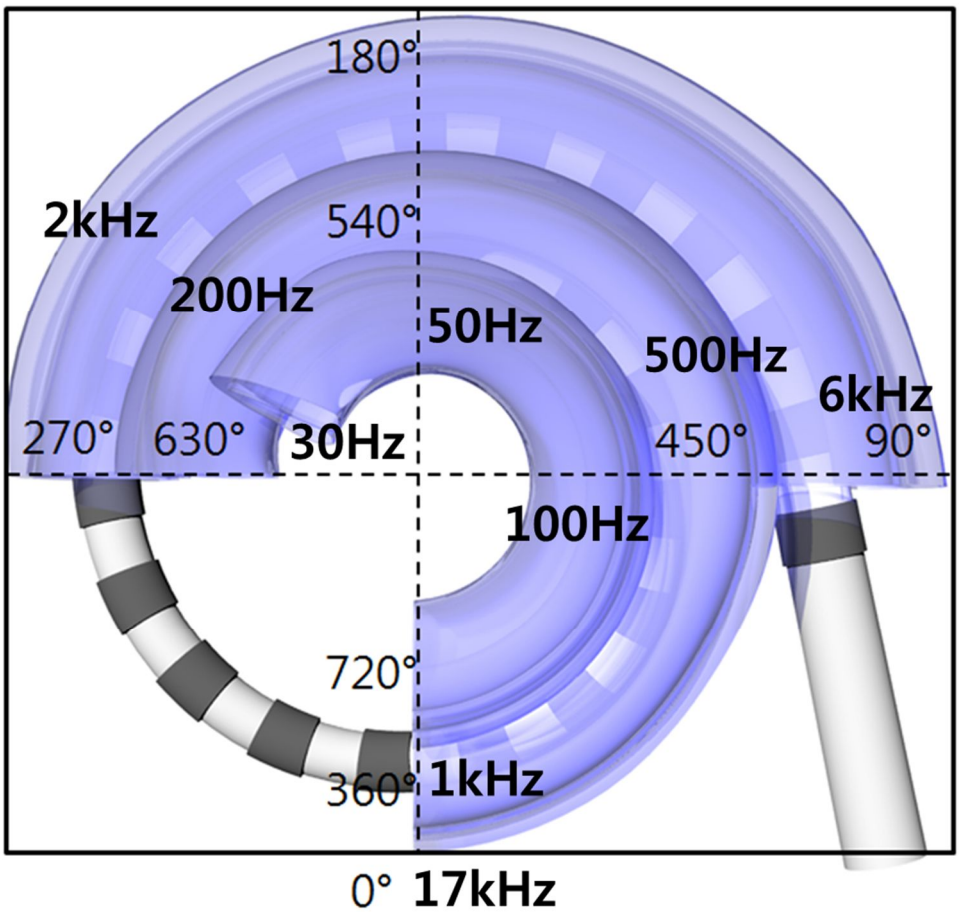

Figure 4.10 Greenwood Frequency-to-Place Map.

4.5.1 Uniform Stiffness of Reinforcement (LCP layers)

As discussed in section 4.3, the mechanical property of the LCP-based intracochlear electrode array is dominated by the LCP structure in silicone elastomer. The insertion force increases as an intracochlear electrode array is inserted in deeper region because of the increasing frictional force and reaction force of reinforcement [67]. The wire-based electrode array satisfies this requirement as the number of wires increases as the number of channel-interconnection increases at the basal region. Likewise, by varying the number of LCP layers in specific area, the stiffness of the LCP-based intracochlear electrode can be controlled so that it has softer tip and stiffer base.

4.5.2 Dimension

As shown in figure 4.11, typical shape of cross-sectioned human cochlea, the cross-sectional area of scala tympani decreases to the apex. The straight electrode arrays are inserted along the lateral wall of scala tympani, the shape and the dimension of the lateral wall should affects the insertion force of proceeding intracochlear electrode array. The dimensions of the conventional electrode array increases as the number of interconnection wire increases, results in large diameter of cross-sectioned area of the electrode array. At the basal turn, as shown in figure 4.11, the length of cross-sectioned lateral wall is relatively longer than that of middle turn. Moreover, the shape of the lateral wall of scala-tympani at apex becomes sharper than decrease of cross-sectional area of scala tympani. This may affects more to the increasing insertion force of deeply inserted intracochlear

electrode array. To overcome this, highly finer intracochlear electrode array should be employed. Moreover, the shape of silicone carrier has to be engineered according to the sharpened lateral wall of scala tympani in the higher turn. In a sense, the application of micro-fabrication process to the intracochlear electrode array is promising technology to achieve the requirements. And, the suggested LCP-based intracochlear electrode array is the first prototype which has enormous potential for development.

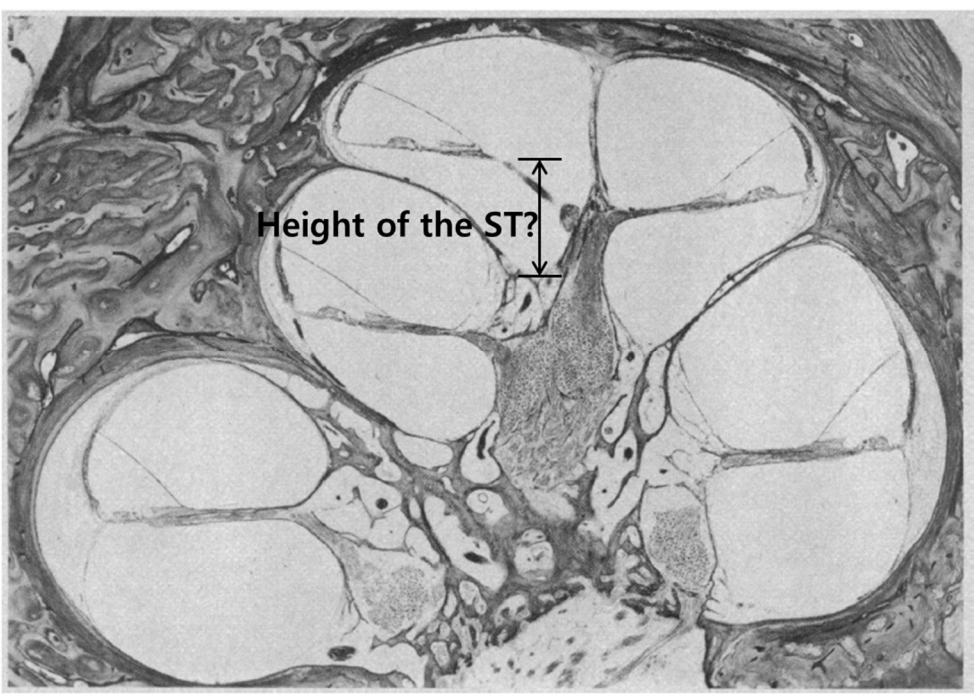

Figure 4.11 Typical Shape of Cross-Sectioned Human Cochlea [68].

Chapter V

Conclusion

In the present study, we developed an LCP-based cochlear electrode array using an advanced LCP-based micro-fabrication process. Through a novel mounting method of LCP film on silicon wafer, the flatness of the LCP surface was enhanced, resulted in higher resolution than conventional LCP-based micro-fabrication process. Based on this, an LCP-based intracochlear electrode array was developed. The sharp edges of the LCP-based electrode array were encapsulated by silicone elastomer carrier. For fine and easy alignment of the LCP-based electrode array to an elastomeric encapsulation without any additional ablation process for site opening, a novel mold design and molding method were suggested, enabled self-aligned micro-molding process. The wavy structure of LCP electrode array obtained from the molding process helped decrease the reaction force of bending LCP film.

The LCP-based cochlear electrode array provides suitable electrochemical properties for electrical stimulation. A 16-channel interconnection was realized on LCP film. The insertion and extraction forces of the LCP-based electrode array were 47 % and 69 %, respectively, of the insertion force and extraction force of a wire-based electrode array, which implies that the present LCP-based electrode array can be inserted with less trauma than a conventional wire-based electrode array.

In the temporal bone study results of LCP-based electrode arrays, two cases of human temporal bone study results showed no observable trauma, whereas three cases showed a rupture of the basilar membrane. The insertion depths were 405°. These results show that the developed LCP-based cochlear electrode array is

applicable to human clinical use.

References

[1] D. F. Williams, "On the mechanisms of biocompatibility," *Biomaterials,* vol. 29, pp. 2941-53, Jul 2008.

[2] D. Williams, "Revisiting the definition of biocompatibility," *Medical device technology,* vol. 14, pp. 10-3, Oct 2003.

[3] A. Colas and J. Curtis, "Silicone biomaterials: history and chemistry," *Biomaterials Science: An Introduction to Materials in Medicine. Eds: Rutner BD, Hoffman AS, Schoen FJ, Lemons JE (eds.),* pp. 80-86, 2004.

[4] C. Namsun, Y. Soonki, and K. Sohee, "A Largely Deformable Surface Type Neural Electrode Array Based on PDMS," *Neural Systems and Rehabilitation Engineering, IEEE Transactions on,* vol. 21, pp. 544-553, 2013.

[5] K. G. Klemic, J. F. Klemic, M. A. Reed, and F. J. Sigworth, "Micromolded PDMS planar electrode allows patch clamp electrical recordings from cells," *Biosensors & bioelectronics,* vol. 17, pp. 597-604, Jun 2002.

[6] D. C. Rodger, W. Li, H. Ameri, A. Ray, J. D. Weiland, M. S. Humayun, and Y.-C. Tai, "Flexible parylene-based microelectrode technology for intraocular retinal prostheses," in *Nano/Micro Engineered and Molecular Systems, 2006. NEMS'06. 1st IEEE International Conference on*, 2006, pp. 743-746.

[7] P. J. Rousche, D. S. Pellinen, D. P. Pivin, Jr., J. C. Williams, R. J. Vetter, and D. R. kirke, "Flexible polyimide-based intracortical electrode arrays

with bioactive capability," *Biomedical Engineering, IEEE Transactions on,* vol. 48, pp. 361-371, 2001.

[8] B. Rubehn, C. Bosman, R. Oostenveld, P. Fries, and T. Stieglitz, "A MEMS-based flexible multichannel ECoG-electrode array," *Journal of neural engineering,* vol. 6, p. 036003, 2009.

[9] R. DeIasi and J. Russell, "Aqueous degradation of polyimides," *Journal of applied polymer science,* vol. 15, pp. 2965-2974, 1971.

[10] S. Murray, C. Hillman, and M. Pecht, "Environmental aging and deadhesion of polyimide dielectric films," *TRANSACTIONS-AMERICAN SOCIETY OF MECHANICAL ENGINEERS JOURNAL OF ELECTRONIC PACKAGING,* vol. 126, pp. 390-397, 2004.

[11] *Vectra® Liquid Crystal Polymer*: Ticona GmbH Corporation, 2007.

[12] S. H. B. Seung Woo Lee, Joon Soo Jeong, Kyung Sik Eom, Jong-Mo Seo, Hum Chung, Sung June Kim, "Monolithically Encapsulated Retinal Implant System using Liquid Crystal Polymers," presented at the Neural Interface Conference 2010, Long Beach Convention Center, Long Beach, CA, USA, 2010.

[13] E. C. Culbertson, "A new laminate material for high performance PCBs: liquid crystal polymer copper clad films," in *Electronic Components and Technology Conference, 1995. Proceedings., 45th*, 1995, pp. 520-523.

[14] R. N. Dean, J. Weller, M. J. M. J. Bozack, C. L. Rodekohr, B. Farrell, L. Jauniskis, J. Ting, D. J. Edell, and J. F. Hetke, "Realization of Ultra Fine Pitch Traces on LCP Substrates," *Components and Packaging*

Technologies, IEEE Transactions on, vol. 31, pp. 315-321, 2008.

[15] C. J. Lee, S. J. Oh, J. K. Song, and S. J. Kim, "Neural signal recording using microelectrode arrays fabricated on liquid crystal polymer material," *Materials Science and Engineering: C,* vol. 24, pp. 265-268, 2004.

[16] S. W. Lee, K. S. Min, J. Jeong, J. Kim, and S. J. Kim, "Monolithic Encapsulation of Implantable Neuroprosthetic Devices Using Liquid Crystal Polymers," *Ieee Transactions on Biomedical Engineering,* vol. 58, Aug 2011.

[17] S. W. Lee, J. M. Seo, S. Ha, E. T. Kim, H. Chung, and S. J. Kim, "Development of Microelectrode Arrays for Artificial Retinal Implants Using Liquid Crystal Polymers," *Investigative Ophthalmology & Visual Science,* vol. 50, pp. 5859-5866, Dec 2009.

[18] J. K. Scott Corbett, Tim Johnson, "Polymer-Based Microelectrode Arrays," in *Materials Research Society Symposium*, 2006.

[19] D. C. Thompson, M. M. Tentzeris, and J. Papapolymerou, "Packaging of MMICs in multilayer LCP substrates," *Microwave and Wireless Components Letters, IEEE,* vol. 16, pp. 410-412, 2006.

[20] K. Jayaraj and B. Farrell, "Liquid Crystal Polymers & Their Role in Electronic Packaging," *Advancing Microelectronics,* vol. 25, pp. 15-18, 1998.

[21] D. J. Edell and B. Farrell, "Implantable devices having a liquid crystal polymer substrate," ed: Google Patents, 2003.

[22] X. Wang, J. Engel, and C. Liu, "Liquid crystal polymer (LCP) for MEMS:

processes and applications," *Journal of Micromechanics and Microengineering,* vol. 13, p. 628, 2003.

[23] J. R. Ketterl, J. P. Yarno, S. S. Corbett III, and T. R. Clary, "Bio-implant and method of making the same," ed: Google Patents, 2004.

[24] S. S. Corbett III, T. J. Johnson, B. M. Clopton, F. A. Spelman, J. A. Strole, and J. R. Ketterl, "Method of making high contact density electrode array," ed: Google Patents, 2004.

[25] V. V. Keesara, D. M. Durand, and C. A. Zorman, "Fabrication and characterization of flexible, microfabricated neural electrode arrays made from liquid crystal polymer and polynorbornene," in *Materials Research Society Symposium Proceedings*, 2006.

[26] K. Wang, C.-C. Liu, and D. M. Durand, "Flexible nerve stimulation electrode with iridium oxide sputtered on liquid crystal polymer," *Biomedical Engineering, IEEE Transactions on,* vol. 56, pp. 6-14, 2009.

[27] R. Dean, J. Weller, M. J. Bozack, C. L. Rodekohr, B. Farrell, L. Jauniskis, J. Ting, D. J. Edell, and J. F. Hetke, "Realization of ultra fine pitch traces on LCP substrates," *Components and Packaging Technologies, IEEE Transactions on,* vol. 31, pp. 315-321, 2008.

[28] G. Zou, H. Gronqvist, J. P. Starski, and J. Liu, "Characterization of liquid crystal polymer for high frequency system-in-a-package applications," *Advanced Packaging, IEEE Transactions on,* vol. 25, pp. 503-508, 2002.

[29] N. Kingsley, S. K. Bhattacharya, and J. Papapolymerou, "Moisture lifetime testing of RF MEMS switches packaged in liquid crystal polymer,"

Components and Packaging Technologies, IEEE Transactions on, vol. 31, pp. 345-350, 2008.

[30] L. Jauniskis, B. Farrell, A. Harvey, and S. Kennedy, "LCP PCB-based Packaging for High-Performance Protection," *Advanced Packaging,* vol. 10, pp. 40-42, 2006.

[31] Q. Bai and K. D. Wise, "Single-unit neural recording with active microelectrode arrays," *Biomedical Engineering, IEEE Transactions on,* vol. 48, pp. 911-920, 2001.

[32] K. Cheung, G. Lee, K. Djupsund, Y. Dan, and L. P. Lee, "A new neural probe using SOI wafers with topological interlocking mechanisms," in *Microtechnologies in Medicine and Biology, 1st Annual International, Conference On. 2000*, 2000, pp. 507-511.

[33] P. Norlin, M. Kindlundh, A. Mouroux, K. Yoshida, and U. G. Hofmann, "A 32-site neural recording probe fabricated by DRIE of SOI substrates," *Journal of Micromechanics and Microengineering,* vol. 12, p. 414, 2002.

[34] T. H. Yoon, E. J. Hwang, D. Y. Shin, S. I. Park, S. J. Oh, S. C. Jung, H. C. Shin, and S. J. Kim, "A micromachined silicon depth probe for multichannel neural recording," *Biomedical Engineering, IEEE Transactions on,* vol. 47, pp. 1082-1087, 2000.

[35] S. J. Oh, J. K. Song, and S. J. Kim, "Neural interface with a silicon neural probe in the advancement of microtechnology," *Biotechnology and Bioprocess Engineering,* vol. 8, pp. 252-256, 2003.

[36] S. J. Oh, J. K. Song, J. W. Kim, and S. J. Kim, "A high-yield fabrication

process for silicon neural probes," *Biomedical Engineering, IEEE Transactions on,* vol. 53, pp. 351-354, 2006.

[37] D. Greitz, R. Wirestam, A. Franck, B. Nordell, C. Thomsen, and F. Ståhlberg, "Pulsatile brain movement and associated hydrodynamics studied by magnetic resonance phase imaging," *Neuroradiology,* vol. 34, pp. 370-380, 1992.

[38] D. J. Edell, V. Toi, V. M. McNeil, and L. Clark, "Factors influencing the biocompatibility of insertable silicon microshafts in cerebral cortex," *Biomedical Engineering, IEEE Transactions on,* vol. 39, pp. 635-643, 1992.

[39] K. Lee, A. Singh, J. He, S. Massia, B. Kim, and G. Raupp, "Polyimide based neural implants with stiffness improvement," *Sensors and Actuators B: Chemical,* vol. 102, pp. 67-72, 2004.

[40] S. Takeuchi, D. Ziegler, Y. Yoshida, K. Mabuchi, and T. Suzuki, "Parylene flexible neural probes integrated with microfluidic channels," *Lab on a Chip,* vol. 5, pp. 519-523, 2005.

[41] B. Wester, R. Lee, and M. LaPlaca, "Development and characterization of in vivo flexible electrodes compatible with large tissue displacements," *Journal of neural engineering,* vol. 6, p. 024002, 2009.

[42] T. D. Y. Kozai and D. R. Kipke, "Insertion shuttle with carboxyl terminated self-assembled monolayer coatings for implanting flexible polymer neural probes in the brain," *Journal of neuroscience methods,* vol. 184, pp. 199-205, 2009.

[43] S. E. Lee, S. B. Jun, H. J. Lee, J. Kim, S. W. Lee, C. Im, H. C. Shin, J. W.

Chang, and S. J. Kim, "A flexible depth probe using liquid crystal polymer," *IEEE transactions on bio-medical engineering,* vol. 59, pp. 2085-94, Jul 2012.

[44] S. Corbett, T. Johnson, and J. Ketterl, "Polymer-based microelectrode arrays," in *MATERIALS RESEARCH SOCIETY SYMPOSIUM PROCEEDINGS*, 2006, p. 46.

[45] R. S. B. Bonham, S. Corbett, T. Johnson, S. Rebscher, M. Carson, F. Spelman, B. Clopton, "Reducing Channel Interaction through Multi-Polar Stimulation: Combining Tripolar and Monopolar Methods with High-Density Arrays," presented at the Conference on Implantable Auditory Prostheses, Asilomar, California, 2005.

[46] C. L. V. Byers, CA), Loeb, Gerald E. (Clarksburg, MD), Merzenich, Michael M. (San Francisco, CA), Rebscher, Stephen J. (San Francisco, CA), "Intracochlear electrode array," United States Patent, 1989.

[47] C. L. V. Byers, CA), Loeb, Gerald E. (Clarksburg, MD), Merzenich, Michael M. (San Francisco, CA), Rebscher, Stephen J. (San Francisco, CA), "Method for making an intracochlear electrode array," United States Patent, 1987.

[48] G. N. Taylor and T. M. Wolf, "Oxygen Plasma Removal of Thin Polymer-Films," *Polymer Engineering and Science,* vol. 20, pp. 1087-1092, 1980.

[49] E. M. Schmidt, M. J. Bak, and P. Christensen, "Laser exposure of Parylene-C insulated microelectrodes," *Journal of neuroscience methods,* vol. 62, pp. 89-92, Nov 1995.

[50] B. J. Gantz, C. Turner, and K. E. Gfeller, "Acoustic plus Electric Speech Processing: Preliminary Results of a Multicenter Clinical Trial of the Iowa/Nucleus Hybrid Implant," *Audiology and Neurotology,* vol. 11, pp. 63-68, 2006.

[51] C. James, K. Albegger, R. Battmer, S. Burdo, N. Deggouj, O. Deguine, N. Dillier, M. Gersdorff, R. Laszig, T. Lenarz, M. M. Rodriguez, M. Mondain, E. Offeciers, Á. R. Macías, R. Ramsden, O. Sterkers, E. Von Wallenberg, B. Weber, and B. Fraysse, "Preservation of residual hearing with cochlear implantation: How and why," *Acta Oto-laryngologica,* vol. 125, pp. 481-491, 2005.

[52] H. Skarzynski and R. Podskarbi-Fayette, "A new cochlear implant electrode design for preservation of residual hearing: a temporal bone study," *Acta Oto-laryngologica,* vol. 130, pp. 435-442, 2010.

[53] S. J. Rebscher, A. Hetherington, B. Bonham, P. Wardrop, D. Whinney, and P. A. Leake, "Considerations for design of future cochlear implant electrode arrays: electrode array stiffness, size, and depth of insertion," *Journal of rehabilitation research and development,* vol. 45, pp. 731-47, 2008.

[54] D. W. Kennedy, "Multichannel intracochlear electrodes: mechanism of insertion trauma," *The Laryngoscope,* vol. 97, pp. 42-49, 1987.

[55] A. A. Eshraghi, N. W. Yang, and T. J. Balkany, "Comparative study of cochlear damage with three perimodiolar electrode designs," *The Laryngoscope,* vol. 113, pp. 415-419, 2003.

[56] P. Wardrop, D. Whinney, S. J. Rebscher, J. T. Roland, Jr., W. Luxford, and P. A. Leake, "A temporal bone study of insertion trauma and intracochlear position of cochlear implant electrodes. I: Comparison of Nucleus banded and Nucleus Contour electrodes," *Hearing research,* vol. 203, pp. 54-67, May 2005.

[57] J. Lee, J. B. Nadol, Jr., and D. K. Eddington, "Factors associated with incomplete insertion of electrodes in cochlear implant surgery: a histopathologic study," *Audiology & neuro-otology,* vol. 16, pp. 69-81, 2011.

[58] B. Bhushan, "Adhesion and stiction: Mechanisms, measurement techniques, and methods for reduction," *Journal of Vacuum Science & Technology B,* vol. 21, pp. 2262-2296, Nov-Dec 2003.

[59] F. W. DelRio, M. P. de Boer, J. A. Knapp, E. D. Reedy, P. J. Clews, and M. L. Dunn, "The role of van der Waals forces in adhesion of micromachined surfaces," *Nature materials,* vol. 4, pp. 629-634, 2005.

[60] M. Coleman, "FLEX Electrodes: Design Matters for Atraumaticity and Hearing Preservation," *The Hearing Journal,* 2012.

[61] J. T. Roland, "A Model for Cochlear Implant Electrode Insertion and Force Evaluation: Results with a New Electrode Design and Insertion Technique," *The Laryngoscope,* vol. 115, pp. 1325-1339, 2005.

[62] C. Jolly, J. Mueller, S. Helbig, and S. Usami, "New trends with cochlear implant electrodes," *Otology Japan,* vol. 20, pp. 239-246, 2010.

[63] D. D. Greenwood, "Critical bandwidth and consonance in relation to

cochlear frequency-position coordinates," *Hearing research,* vol. 54, pp. 164-208, Aug 1991.

[64] M. F. Dorman, T. Spahr, R. Gifford, L. Loiselle, S. McKarns, T. Holden, M. Skinner, and C. Finley, "An electric frequency-to-place map for a cochlear implant patient with hearing in the nonimplanted ear," *Journal of the Association for Research in Otolaryngology : JARO,* vol. 8, pp. 234-40, Jun 2007.

[65] Q. J. Fu, R. V. Shannon, and J. J. Galvin, 3rd, "Perceptual learning following changes in the frequency-to-electrode assignment with the Nucleus-22 cochlear implant," *The Journal of the Acoustical Society of America,* vol. 112, pp. 1664-74, Oct 2002.

[66] K. Yukawa, L. Cohen, P. Blamey, B. Pyman, V. Tungvachirakul, and S. O'Leary, "Effects of insertion depth of cochlear implant electrodes upon speech perception," *Audiology and Neurotology,* vol. 9, pp. 163-172, 2004.

[67] S. J. Rebscher, M. Heilmann, W. Bruszewski, N. H. Talbot, R. L. Snyder, and M. M. Merzenich, "Strategies to improve electrode positioning and safety in cochlear implants," *Biomedical Engineering, IEEE Transactions on,* vol. 46, pp. 340-352, 1999.

[68] M. Igarashi, M. Takahashi, and B. R. Alford, "Cross-sectional area of scala tympani in human and cat," *Archives of otolaryngology,* vol. 102, pp. 428-9, Jul 1976.

국문 초록

신경 인터페이스로서, 액정폴리머 (Liquid Crystal Polymer)는 화학적 안전성, 낮은 흡습성 및 낮은 수분 침투율로 인해 가혹한 몸 속 환경에 오랜 기간동안 이식할 수 있는 물질이다. 지금까지 발표된 액정폴리머 기반 신경 인터페이스는 반도체공정, 열 압착, 레이저 가공 등의 과정을 거친다. 지금까지 발표된 액정 폴리머 기반의 신경 전극에 대한 연구에서는 높은 녹는점을 갖는 액정 폴리머와 낮은 녹는점을 가진 액정 폴리머를 이용하였다. 높은 녹는점을 갖는 액정 폴리머는 마이크로 패턴을 위한 기판과 그 기판을 패키지 하기 위한 것인 반면, 낮은 녹는 점을 갖는 액정 폴리머는 기판과 패키지 사이의 접착을 위해 사용되었다. 열 압착 공정 후 레이저를 이용하여 전극의 외곽선을 잘라 낸다. 이전에 발표된 연구들에서는 50 μm의 미세 도선을 패터닝할 수 있었는데, 이는 반도체 공정의 이점을 충분히 활용하지 못한 결과이다. 그리고 레이저 가공과 열 압착 공정에서 발생되는 정렬 오차 또한 확실하게 정립이 되지 않아서 액정 폴리머 기반의 신경 인터페이스의 생산성을 높이기 위해 최적화된 공정 조건이 확립되어야 한다.

본 연구에서는 액정 폴리머 기반 신경 인터페이스의 제작을 위한 진보된 공정 방법에 대해 논하였다. 이전의 연구들에서는 반도체 미세공정에 액정 폴리머를 이용하기 위하여 실리콘 웨이퍼

위에 액정 폴리머를 부착할 때 감광제 (photoresist)를 이용하였는데, 시간이 지남에 따라 감광제에서 발생되는 기포에 의해 표면의 편평도(flatness)가 낮아지게 된다. 이는 공정의 해상도를 낮추는데 기여하게 된다. 이를 극복하기 위하여 실리콘 엘라스토머를 이용한 실리콘 웨이퍼와 액정 폴리머 부착 방법을 개발하였고, 이를 통하여 이전에 비해 향상된 편평도를 얻을 수 있었다. 그 결과로 10 μm 의 미세 도선을 20 μm 간격으로 공정할 수 있게 되었다. 또한 레이저 가공과 열 압착 공정의 정렬 오차를 측정하여 전극 디자인을 최적화하였다.

그리고, 앞서 서술한 공정 방법을 기반으로 매우 유연한 인공와우 전극을 개발하였다. 기존에 발표된 액정 폴리머 기반의 인공와우 전극은 사용한 액정 폴리머의 두께도 50 μm 로 매우 두꺼웠으며, 총 250 × 250 μm^2 의 단면을 갖는 매우 딱딱한 성질을 가지고 있었기 때문에 사람 임상용으로 사용할 수 없었다. 본 연구에서는 25 μm 두께의 액정 폴리머 두 장만을 이용하여 16 채널의 전극 어레이를 만들었다. 완성된 액정 폴리머 구조물의 두께는 은 기존에 발표된 액정 폴리머 기반 인공와우 전극의 두께의 1/5 로서, 매우 유연한 성질을 갖는다. 더 높은 유연성을 갖도록 하기 위해서, 기판과 패키지에 해당하는 액정 폴리머는 도선과 전극을 유지할 수 있을 정도만 남겨 놓고 최대한 얇게 가공하였다. 얇아진 액정 폴리머 기반 전극 어레이의 날카로운 측면으로부터 와우의 주변 조직을 보호하기 위해 의료용 실리콘 엘라스토머를 이용하여 액정 폴리머 전극 어레이를 감쌌다. 이를 위하여 자가 정렬

이 가능한 미세 몰딩 공정을 개발하였다. 완성된 전극의 크기는 끝부분(tip)과 시작부분(base)의 단면이 각각 0.5 mm 와 0.8 mm 의 지름을 갖는 반원 모양이며 길이는 28 mm 이다.

이 전극이 실제 사람 임상용으로 사용될 수 있는지를 판단하기 위해 전기화학적, 기계적 성질을 측정하였는데, 전하 저장 용량(Charge Storage Capacity)과 1 kHz에서의 임피던스가 각각 38.0 mC/cm2 과 391 Ω 이었다. 투명한 와우 모형에 개발된 전극을 삽입하면서 측정한 와우창 (Round Window)으로부터 8 mm 지점에서의 삽입 힘은 8.2 mN 이었고 최대 적출 힘은 110.4 mN 이었다. 사람의 측두골을 이용한 와우 삽입 실험에서 관찰한 결과를 통해 평균 삽입 각도는 405° 로 측정 되었고, 다섯건의 삽입 실험 결과 두 건에서 조직의 손상 없이 전극이 삽입이 되었으며, 나머지 세 건에서 기저막이 찢어진 것을 관찰하였다.

주요어: 인공와우, 액정폴리머, 인공와우 전극, 유연한 신경 전극, 폴리머 기반 신경보철, 강성조절

학 번: 2009-30914

감사의 글

먼저 무사히 박사과정을 마치고 지금까지의 길로 인도하신 하나님께 감사 드립니다. 박사과정 공부를 하면서 너무나 많은 분들께 도움을 받아 그 내용을 일일이 이 지면에 적어낼 수 없겠지만, 간략하게나마 감사의 마음을 표하고 싶습니다. 먼저 석사과정부터 지금까지 지도해 주신 김성준 교수님께 감사드립니다. 연구가 연구에만 그치지 않고, 무엇인가 세상을 이롭게 하고자 끊임없이 매진하시고 그런 방향으로 이끌어 주셔서 연구를 하는 목적을 알게 해 주셨습니다. 건강하시고 항상 변함없는 모습으로 지도해 주시기를 기도하겠습니다. 연구실 동기 김진호씨 먼저 졸업해서 미안합니다. 좋은 결과로 빨리 졸업하게 기도하겠습니다. 졸업을 준비하고 있는 김정훈씨도 잘 마무리하고 원하는 대로 앞길이 잘 열리길 바랍니다. 항상 열심인 이성은씨 가족 모두 건강하길 바라고 열심히 연구하는 만큼 좋은 성과 있었으면 좋겠습니다. 방장을 하느라 고생한 정준수씨, 열심히 하는 모습이 보기 좋습니다. 앞으로 잘되리라 믿어 의심치 않습니다. 순수하고 착한 박정환씨 귀여운 모습을 너무 많이 놀려 미안합니다. 애정이 없었다면 그렇게 놀리지 못했으리라는 것 알아주었으면 좋겠습니다. 신수원씨는 더 건강해지고 연구도 잘 진행되어 강철체력으로 연구실을 이끌 수 있도록 기도하겠습니다. 이번에 함께 졸업하게 된 이근재씨에게 먼저 축하드리고, 회사에 가서도 인정받는 엔지니어가 되길 바랍니다. 인공와우 연구를 이어 받게 된 권태목씨는 특유의 성실함으로 기존의 결과보다 훨씬 멋진 결과를 얻어낼 수 있을거라 믿어 의심치 않습니다. 연구실 생활을 함께 오래 하지 못한 신입생들인 김채빈, 안승희, 서정민씨, 지도교수님과 선배들을 전적으로 믿고 잘 따르면 좋은 연구 결과가 있을 테니 아무쪼록 좋은 연구자로 성장하기를 바랍니다.

이미 졸업하신 선배님들과 후배님들에게도 감사의 인사를 하고 싶습니다. 석사 신입생일 때부터 많은 도움의 말씀을 주시고 연구에 대한 열정을 가르쳐 주신 박세익

박사님과 전상범 교수님께 감사드립니다. 팹에서 퍼니스를 돌리느라 하얗게 지새운 밤들이 밑거름이 되어 오늘이 있을 수 있었습니다. 망막팀의 일원으로 연구할 때 많이 가르쳐주신 주경애 박사님 김의태 박사님께도 감사 드립니다. 뉴로바이오시스에서 많은 도움과 조언을 주신 안순관 박사님께도 감사드립니다. 개발에 힘쓰고 계신 인공와우 시스템이 하루 빨리 많은 환자들에게 소리를 찾아 줄 수 있도록 기도하겠습니다. 저의 첫번째 칩을 설계하는 데 많은 도움을 주신 이중재 박사님, 정신적인 면이나 연구적인 면에서 너무나 많은 도움을 주신 점 감사드립니다. 앞으로도 자주 뵙고 저와 선배님 만큼이나 가족들도 서로 의지하고 도움을 주고 받는 좋은 관계를 지속했으면 좋겠습니다. 이제 직장상사로 모시게 될 송종근 박사님, 연구실에서도 시간 가는 줄 모르고 많은 조언을 해주신 것 감사드립니다. 앞으로도 더 좋은 연구로 회사와 팀에 도움이 될 수 있게 열심히 하겠습니다. 석사과정 때 많은 공정 연습을 할 수 있도록 해 주신 변경민 교수님 감사합니다. 지금도 뵐 때마다 좋은 말씀 많이 해 주셔서 도움이 많이 된답니다. 이종환 박사님, 항상 너무나 스마트한 모습으로 주눅들게 만드셨지만 그 모습을 보고 너무나 많은 것을 배웠습니다. 이승우 박사, 연구실 선배로서 친구로서 많은 도움을 주었고 무엇보다 이승우 박사가 이룩해 놓은 업적이 없었다면 저의 연구가 진행되지 않았을 것임을 알기에 감사합니다. 칩설계 할 때 많은 도움을 주었고 선배답게 중심을 잘 잡아준 이태형 박사에게도 감사합니다. 앞으로 예쁜 아기도 낳고 화목한 가정 되길 바라고 하는 일도 더 잘 풀리길 기도하겠습니다. 사수로서 많은 도움을 주었던 김신애 박사에게도 감사합니다. 김신애 박사도 다복하고 화목한 가정이 되길 기도하고 아무쪼록 원하는 직장에 잘 자리잡기를 바라겠습니다. 김진원 박사님께 항상 온화한 모습과 친절한 모습에 많은 감명을 받았습니다. 연구실에서 뵈었던 것에 참 많은 위안을 받았고 도움을 받았습니다. 그리고 항상 여유있으시던 이원희 박사님도 감사합니다. 이전에는 흥분하기 쉽고 토론 중에 얼굴을 붉히는 일이 많은 성격이었는데, 박사님과 많은 토론을 하면서 그러한 성격을 많이

고칠 수 있었습니다. 아무쪼록 두 분도 원하시는 곳에 잘 자리를 잡으실 수 있도록 기도하겠습니다. 그밖에 정세훈씨, 강수아씨, 전태호씨, 최승호씨, 장성민씨, 장재명씨, 김정태씨, 문효원씨, 김진규씨도 감사 인사를 길게 하고 싶지만, 지면이 허락하지 않아 그리 못하는 것 너그러이 용서해 주시기 바랍니다.

뉴로바이오시스의 임직원 여러분에게도 감사드립니다. 이홍주 이사님, 도정옥 대리님, 김찬희 대리, 임정우 과장, 김두희 과장, 문창식씨, 김상현씨도 감사합니다. 그리고 연구를 도와 주신 오승하 교수님, 장진우 교수님, 신형철 교수님께도 감사 인사 드립니다. 오승하 교수님께서 많은 기여를 해 주셔서 논문을 쓸 수 있었고, 졸업도 할 수 있었던 점 항상 잊지 않고 언젠가 꼭 좋은 연구로 도움을 드릴 수 있도록 열심히 하겠습니다. 끝까지 심뇌부 자극기 팀에서 장진우 교수님께 큰 도움을 드리지 못한 점 죄송합니다. 그래도 장진우 교수님께서 도와 주신 덕에 신경 조절 시스템 논문을 완성할 수 있었습니다. 아까도 감사 인사를 드렸지만, 전상범 교수님께서 논문 작성을 많이 도와 주신 덕에 저널 논문을 올해 세 편이나 작성할 수 있었습니다. 측두골 삽입 실험을 도와주신 박민현 선생님과 이호선 선생님께도 감사 드립니다. 쥐 실험을 도와 준 김진형씨에게도 감사 인사를 전합니다.

무엇보다 지금까지 믿고 뒷바라지 해 준 아내 이진희씨에게 감사드립니다. 못난 남편의 부족한 성격이나 짜증도 받아 주고, 변함 없는 사랑으로 묵묵히 애써 주신 점 너무나도 감사 드립니다. 잘 성장하고 있는 민대찬군 민혜원양에게도 감사합니다. 또한 지금까지 키워주시고 응원해 주신 아버지 어머니, 부족한 사위를 위해 기도해 주시고 지원을 아끼지 않아 주신 장인어른 장모님께도 감사 드립니다.

이 외에도 감사드릴 분들이 너무나 많이 있지만, 더 훌륭한 사람으로 성장함으로써 은혜에 보답하고자 합니다. 이 논문이 나올 수 있도록 도와주신 모든 분들께 감사드립니다.